The Zedong Window: A record of superposed Tertiary convergence in southeastern Tibet

T. Mark Harrison, An Yin, Marty Grove, and Oscar M. Lovera

Department of Earth and Space Sciences and Institute of Geophysics and Planetary Physics, University of California, Los Angeles

F. J. Ryerson

Institute of Geophysics and Planetary Physics, Lawrence Livermore National Laboratory, Livermore, California

Xinhua Zhou

Institute of Geology, Academia Sinica, Beijing

Abstract. Determining the timing, magnitude, and location of deformation due to the Indo-Asian collision is widely acknowledged as an important step in understanding how the lithosphere responds during continental collision. A puzzling result of geological investigations of the Lhasa Block over the past 2 decades has been the apparent lack of significant Tertiary deformation there. Perhaps the most important structural feature of the Lhasa Block is the south directed Gangdese Thrust System, which developed along its southern edge. The thrust system, which separates the Andean-type batholith of southern Asia from rocks of Indian affinity, is obscured at most locations across southeastern Tibet by back thrusts of the younger, north directed Renbu Zedong Thrust System. The best documented site where both thrusts are exposed occurs near Zedong (Zedong Window). Systematic geochronologic analyses were conducted in this area. U-Pb zircon dating of three samples of a synkinematically to postkinematically deformed hanging wall granitoid (the Yaja granodiorite) cut by the Gangdese Thrust indicates a crystallization age of 30.4 ± 0.4 Ma (2σ), thus placing an upper bound on the initiation of the thrust. U-Pb zircon dating of granitoid samples structurally higher in the Gangdese hanging wall yields emplacement ages of 42.5 ± 1.0 Ma and 48.9 ± 0.8 Ma (2σ), similar to other magmatic complexes within the Gangdese arc. Geochemical results are consistent with these plutons forming in the same environment as precollisional intrusions within the Gangdese batholith, suggesting a significant postcollisional input of juvenile heat. The ^{40}Ar/^{39}Ar thermochronology of samples from a vertical section through the hanging wall within the Yaja granodiorite, coupled with results of a numerical thermal model, indicate an average slip rate along the Gangdese Thrust of 7 mm/yr between 30 and 23 Ma and a minimum displacement of ~50 km. Farther east in the Zedong Window, thermal effects produced by later north directed thrust sheets of the Renbu Zedong system appear to have obscured thermal history signatures in the Gangdese hanging wall related to earlier south directed thrusting. Thermochronological results from this region indicate that thermal overprinting related to the north directed thrusting occurred between 25 and 10 Ma, consistent with previous estimates.

1. Introduction

Even prior to the advent of modern geological studies by western scientists [e.g., *Allègre et al.*, 1984], the remarkable and singular nature of the Himalayan/Tibetan orogen drew the attention of geodynamic modelers [e.g., *Bird*, 1978; *Houseman et al.*, 1981]. While early numerical investigations of thin sheet approximations for continental deformation in general predicted that lithospheric thickening due to the Indo-Asian collision should first have occurred in southern Tibet

and then propagated northward [e.g., *England and McKenzie*, 1982], initial reports from geological studies in southern Tibet indicated little or no Tertiary deformation there [e.g., *Chang et al.*, 1986]. Ad hoc theories were advanced to explain why the Andean-type batholith adjacent the suture zone might have escaped collision-related thickening [e.g., *England and Searle*, 1986], but subsequent investigations [e.g., *Pan*, 1993; *Murphy et al.*, 1997] revealed a general lack of significant post collisional deformation throughout the Lhasa Block (Plate 1). The nature of crustal shortening in southern Tibet was clarified only as the evolution of the Indus Tsangpo suture zone (Plate 1) became better understood [*Ratschbacher et al.*, 1994; *Yin et al.*, 1994].

The contact that separates the Gangdese batholith [*Honegger et al.*, 1982; *Schärer et al.*, 1984; *Xu et al.*, 1985; *Xu*,
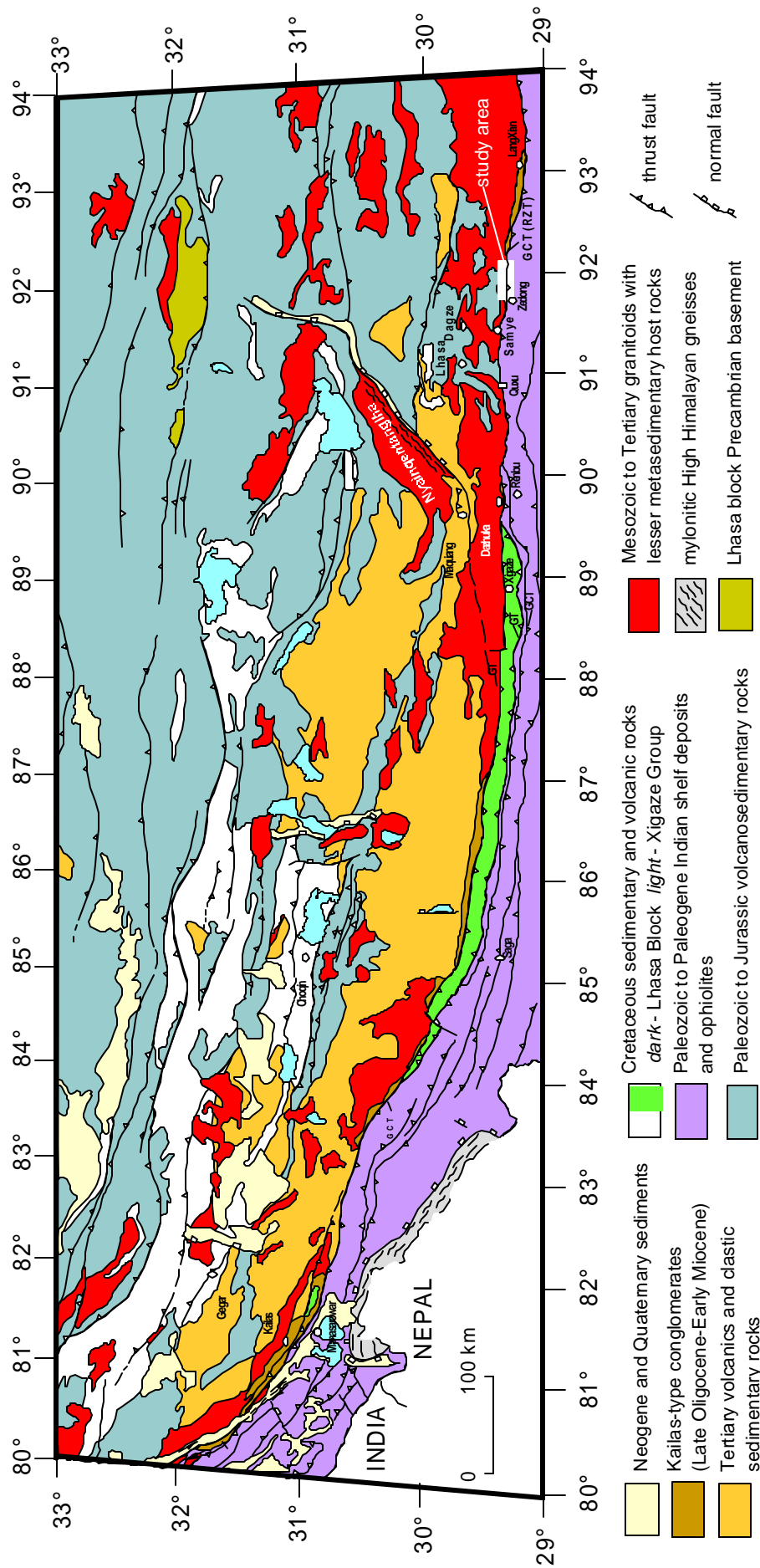
Plate 1. Geologic map of southern Tibet. The Indus Tsangpo suture zone separating Asia from rocks of Indian affinity is largely defined by the Great Counter Thrust, which juxtaposes Paleozoic to Cretaceous Indian shelf deposits against the Cretaceous–Tertiary Gangdese batholith (modified from *Tibetan Bureau of Geology and Mineral Resources* [1982]). GCT, Great Counter Thrust, GT, Gangdese Thrust, RZT, Renbu Zedong Thrust. The location of Plate 2 is indicated by the white box marked "study area".

1990; *Copeland et al.*, 1995; *Quidelleur et al.*, 1997], the Cretaceous-Tertiary magmatic arc that developed along the margin of southern Asian (Plate 1), from metasediments originating on the Indian shelf (Plate 1) is in most locations a north directed thrust [*Yu and Zheng*, 1979; *Burg*, 1983; *Searle et al.*, 1987; *Liu*, 1988; *Kidd et al.*, 1988; *Ratschbacher et al.*, 1994; *Yin et al.*, 1994, 1999]. The Gangdese batholith is broadly characterized by Cretaceous-Paleogene volcanic and hypabyssal rocks west of Renbu (Plate 1), and age-equivalent plutonic rocks east of Renbu that were substantially denuded during the early Miocene [*Copeland et al.*, 1995]. This map relationship indicates differential unroofing along strike: the structural level of pluton exposure east of Renbu is typically ~15 km, whereas the widespread preservation of precollisional volcanic rocks in south central Tibet suggests substantially less denudation west of that location [*Harrison et al.*, 1992]. Spatially corresponding to the preservation of volcanic cover in the central Gangdese belt is the appearance, to the south, of forearc strata of the Xigaze Group (Plate 1).

To explain the observed thermochronological relationships in southeastern Tibet and the preservation of Xigaze Group sediments only in the central portion of the suture zone, *Harrison et al.* [1992] proposed the existence of an earlier, south directed Gangdese Thrust (GT). Displacement along such a feature would have had the dual effects of locally subducting the forearc sediments and thickening, uplifting, and exhuming the overlying portion of the batholith. Almost immediately following the prediction of *Harrison et al.* [1992], the GT was discovered near Zedong [*Yin et al.*, 1992], exposed within a tectonic window created by the north directed thrusts, there known as the Renbu Zedong Thrust System (RZTS) (Plates 1 and 2). *Yin et al.* [1994] traced the Gangdese Thrust northwest of Xigaze (Plate 1), interpreting a south dipping fault there as a back thrust within the hanging wall of the Gangdese Thrust System (GTS). A lower bound on the age of that back thrust of ~18 Ma was obtained from crosscutting relationships. Rapid cooling inferred from reconnaissance $^{40}Ar/^{39}Ar$ thermochronology from samples within a mylonitic shear zone near Zedong suggested that the GT hanging wall was moving up the thrust ramp between about 27 and 23 Ma [*Yin et al.*, 1994]. Assuming that deformation within the Xigaze Group was related to motion on the GTS, *Yin et al.* [1994] estimated a minimum displacement and slip rate of 46±9 km and 12±6 mm/yr, respectively. The geological relationships in the Zedong area are similar in at least two respects to those in far southwestern Tibet. East of Mount Kailas (Plate 1), disappearance of the Xigaze Group strata is again correlated with Early Miocene unroofing, suggesting that the south directed thrusts of the GTS may have been active over at least 1100 km along strike [*Yin et al.*, 1999].

A recent deep crustal seismic reflection profile across southern Tibet imaged features consistent with both the RZTS and the GTS [*Makovsky et al.*, 1996]. The younger RZTS in most locations obscures the GTS, at least partly explaining its late discovery [*Yin et al.*, 1992]. *Quidelleur et al.* [1997] used $^{40}Ar/^{39}Ar$ thermochronology to ascertain that slip was active on the RZTS between 18 and 10 Ma, thereby placing an additional lower bound on the timing of slip along the GT.

We have returned to the Zedong region to more fully investigate the displacement history of the Gangdese Thrust. The approach we have taken is to date the crystallization age of granitoids deformed by slip along the GT and to use detailed $^{40}Ar/^{39}Ar$ thermochronology of samples from vertical sections through the hanging wall to assess the timing of movement of the presently exposed rocks up the thrust ramp. Combined with a thermal model, this approach provides constraints on the timing and magnitude of slip along the GT within the central portion of the Zedong Window. To the east, heating of the Gangdese batholith due to overthrusting by north directed thrusts of the RZTS appears to have obscured the thermal effects of earlier deformation. However, this overprint can be used to further understand the relationship between the two thrust systems and the timing of the change in thrust direction along the suture zone.

2. Geological Setting

The general stratigraphic and structural setting of southeastern Tibet is described by *Yu and Zheng* [1979]. Their map shows that the suture zone across most of southeastern Tibet is defined by a north directed thrust they termed the Yalu Tsangpo Fault, also variously referred to locally as the Great Yalu Tsangpo Deep Fault Zone [*Wang et al.*, 1983], the South Kailas Thrust [*Cheng and Xu*, 1987], Renbu Zedong Thrust [*Yin et al.*, 1994], and the Backthrust System [*Ratschbacher et al.*, 1994]. In recognition of its ubiquity along the entire suture zone, *Yin et al.* [1999] proposed that the orogen scale feature be referred to by its earliest designation, the Great Counter Thrust [*Heim and Gansser*, 1939; *Gansser*, 1964]. Although our observations [*Yin et al.*, 1994, 1999; *Quidelleur et al.*, 1997] confirmed many aspects of the geological framework of *Yu and Zheng* [1979] and *Liu* [1988] in southeastern Tibet, the contact between the Gangdese batholith and Tertiary conglomerates in the Zedong area (Plate 1) is not an unconformity as originally believed but instead is a south directed thrust fault [*Yin et al.*, 1994].

Yin et al. [1999] subsequently described three structural domains in the Zedong Window defined by the north dipping Gangdese and south dipping Renbu Zedong Thrust Systems: the hanging wall of the Gangdese Thrust to the north, the hanging wall of the Renbu Zedong Thrust to the south, and intervening melange overlain by both faults.

2.1. Gangdese Thrust

The hanging wall of the Gangdese Thrust in the Zedong region consists of granitoids of the Gangdese batholith intruded into a sequence of Paleozoic and Mesozoic metasedimentary rocks, Cretaceous volcanoclastics, and granitoid gneiss [*Yu and Zheng*, 1979; *Yin et al.*, 1999]. An otherwise undeformed hornblende-bearing granodiorite which crops out on Yaja Mountain (Plates 2 and 3) is mylonitically deformed along its truncated base by the Gangdese Thrust. The ~200-m-thick shear zone produced within the GT at the base of the Yaja pluton is characterized by fabrics that suggest syndeformational temperatures of at least ~450°C (e.g., crystal plastically deformed feldspars). Structurally higher in the GT hanging wall, granitoids (e.g., the Kangagang granodiorite; Plate 2) are tabular and approximately parallel to foliation (Plates 2 and 3). The subparallel orientation of foliation, relict bedding, and the sill like plutonic bodies within the hanging wall of the Gangdese Thrust all indicate that the present exposure of the Gangdese Thrust, which currently dips at ~30°N (Plates 2 and 3), originated along a shallowly dipping fault and was subsequently steepened by upward motion
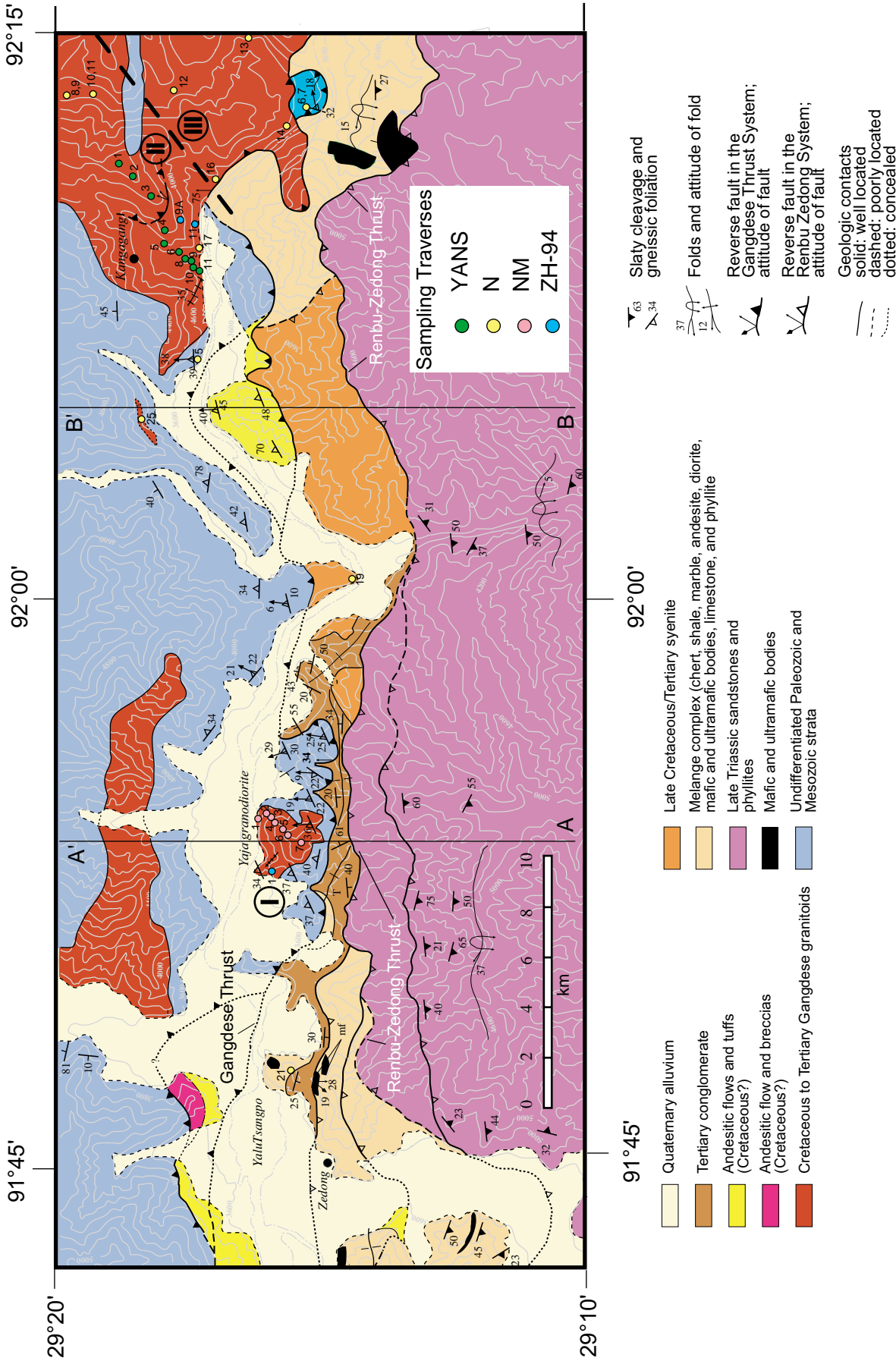
Plate 2. Geologic map of the Zedong area [from *Yin et al.*, 1999]. See Plate 1 for location of mapped area within southern Tibet. Cross sections A-A' and B-B' are shown in Plate 3.

along a thrust ramp. This inferred ramp flat geometry is consistent with a systematically decreased depth of exposure of the Gangdese batholith northward from our study area [*Pan et al.*, 1993; *Copeland et al.*, 1995].

Kinematic indicators within the mylonitic shear zone, composed of marble, granitoid, and schist, all indicate a top to the south sense of shear [*Yin et al.*, 1994, 1999]. The dip angle of the fault varies considerably, from ~30° in the western and central part of the Zedong Window, to 75° ~4 km southeast of Kangagang (Plate 2). We attribute folding and local steepening of the Gangdese Thrust in this eastern domain (Plate 2) to a later deformation, probably in response to movement along the Renbu Zedong Thrust System [*Yin et al.*, 1999].

2.2. Renbu Zedong Thrust

The south dipping Renbu Zedong Thrust System (RZTS) effectively marks the suture in southeastern Tibet [*Yin et al.*, 1994, 1999; *Ratschbacher et al.*, 1994; *Quidelleur et al.*, 1997]. Near Zedong, the RZTS juxtaposes an isoclinally folded sequence of Late Triassic shales and phyllites over melange [*Yin et al.*, 1999]. The fault zone includes several imbricate thrusts in the footwall and hanging wall of the RZTS (Plates 2 and 3). Isoclinal folding within the hanging wall is associated with a south dipping slaty cleavage. Kinematic indicators from within the RZTS fault zone show a top to the north sense of shear deformation. West and east of the map area (Plate 2), rocks of Tethyan affinity have been thrust along the RZTS over the trace of the GT to define the limits of the Zedong Window (Plate 1).

2.3. Footwall of Gangdese and Renbu Zedong Thrusts

Rocks exposed beneath the opposing thrusts include plutonic rocks that are locally thrust over complexly deformed, chert rich melange. Late Cretaceous fossils found in the melange complex [*Yu and Zheng*, 1979] provide an upper bound for the age of the protolith. A >200 m thick sequence of Tertiary conglomerate unconformably overlies both units (Plates 2 and 3). Clasts within the Tertiary conglomerate are dominantly marble and volcanic breccia, with less granitoid detritus [*Yin et al.*, 1999]. *Yu and Zheng* [1979] interpret fossils recovered from this clastic unit to be Oligocene to Miocene.

3. Analytical and Computational Approach

3.1. Sampling

Sample locations are shown in map view in Plate 2. Coordinates are listed in Table 1. Roughly half of the geochronological measurements were performed using 16 granitoid samples obtained along two traverses within the hanging wall of the Gangdese Thrust. The traverses, designated NM (including ZH-1-94) and YANS, provide vertical relief of 750 m and 1200 m, respectively (Table 1). Most of the remaining 18 samples examined were also collected from granitoids within the Gangdese Thrust hanging wall. In general, these samples were obtained close to the base elevation of the region (3500 m) within a 40 km x 10 km region oriented parallel to the strike of the Gangdese Thrust. Four samples (N-6, N-7, N-19, and N-21) were obtained from amphibolite, orthogneiss, syenite, and granodiorite bodies, respectively, from the region beneath the opposing thrusts.

3.2. U-Pb Methods

The UCLA CAMECA ims 1270 ion microprobe was used to determine U-Pb crystallization ages of three granodiorite bodies proximal to the NM and YANS traverses. Zircons from six samples were studied (Plate 2): three from the Yaja granodiorite (NM-1, NM-7, and ZH-1-94), two from the Kangagang granodiorite (YANS-5 and YANS-10), and sample N-9 from the northeasternmost point of the study area (Plate 2). Zircon grains were mounted in epoxy, polished to 0.25 μm diamond paste, and coated with ~100 Å of Au. These analyses utilized a 4-8 nA primary O⁻ beam focused to a ~15 x 25 μm spot. The ion microprobe was operated at a mass resolving power of ~6000 with an energy window of 50 eV. A 5 to 15 eV offset was used for $^{238}U^+$ relative to Pb^+ and UO^+ to compensate for their contrasting energy distributions. Oxygen flooding to a pressure of about 3×10^{-5} torr was employed to increase Pb^+ yields. U-Pb ages were determined by comparison with a working curve defined by measurement of standard zircon AS-3 which yields concordant $^{206}Pb/^{238}U$ and $^{207}Pb/^{235}U$ ages of 1099.1±0.5 Ma by conventional methods [*Paces and Miller*, 1993]. Additional details of analytical methods are given by *Quidelleur et al.* [1997] and *Dalrymple et al.* [1999]. (Complete data tables may be obtained from http://oro.ess.ucla.edu/argon.html.)

3.3. $^{40}Ar/^{39}Ar$ Methods

High purity concentrates of K-feldspar, hornblende, biotite, and muscovite were irradiated at the Ford Reactor, University of Michigan, in three separate sessions (denoted UM75, UM79, and UM82; see Table 1). The J factors determined from Fish Canyon sanidine (27.8 Ma) flux monitors varied between 0.0052 and 0.0068, depending upon the irradiation in question (Table 1). Correction factors for interfering neutron reactions determined from K_2SO_4 and CaF_2 included with the samples are listed in Table 1. In most instances, mica flakes were fused with a continuous 5-W Ar ion laser. All K-feldspar (~25 mg aliquots of ~0.7 mm grains) and amphibole samples (~15 mg aliquots) were step heated in a Ta crucible within a double vacuum furnace. The $^{40}Ar/^{39}Ar$ isotopic measurements were performed using either a VG 3600 or VG 1200S automated mass spectrometer. Heating schedules employed for K-feldspars are described by *Lovera et al.* [1997]. Diffusion parameters calculated from the ^{39}Ar measurements are included in Table 2 of *Lovera et al.* [1997]. Additional experimental details are given by *Harrison et al.* [1991], *McDougall and Harrison* [1999], and *Quidelleur et al.* [1997]. A summary of $^{40}Ar/^{39}Ar$ ages is given in Table 1. (Detailed tabulated results and derivative plots for all argon isotopic analyses calculated using conventional decay constants and isotope abundances are available at http://oro.ess.ucla.edu/argon.html.)

3.4. Geochemical Analyses

Major and trace element concentrations of 11 granitoid samples (9 from the Yaja granodiorite and 2 from the Kangagang granodiorite) were analyzed by Actlabs of Ancaster, Ontario. Powdered samples were mixed with a lithium metaborate/lithium tetraborate flux and fused in an induction furnace. An internal standard was added to the melt that was subsequently dissolved in a 5% nitric acid solution. These solutions were analyzed for major elements using a Thermo

TABLE 1. Summary of ^{40}Ar/^{39}Ar Results

Sample	Rock Type	Elevation m	Longitude	Latitude	Mineral	J-Factor	Total Gas Age, Ma	Weighted Mean Age ±2 σ,Ma	Isochron Age Age±2σ, Ma
NM-1	granodiorite	3500	91° 54.2'	29° 16.2'	Ksp	0.005408[a]	27.3	-	-
NM-1	granodiorite	3500	-	-	Bio	0.005409[a]	29.3	29.2±0.2	28.4±1.6
NM-3	granodiorite	3700	91° 54.2'	29° 15.9'	Bio	0.005412[a]	27.8	27.8±1.0	29.2±3.2
NM-4	granodiorite	3800	91° 54.1'	29° 15.8'	Bio	0.005414[a]	29.1	29.3±0.4	30.1±0.6
NM-4	granodiorite	3800	-	-	Hbd	0.006637[b]	33.8	32.6±1.4	31.5±2.6
NM-5	granodiorite	3950	91° 53.9'	29° 15.7	Bio	0.005416[a]	27.0	27.0±0.4	30.0±1.6
NM-5	granodiorite	3950	-	-	Hbd	0.006636[b]	33.4	33.2±0.8	33.1±1.2
NM-6	granodiorite	4050	91° 53.8'	29° 15.6'	Bio	0.005418[a]	29.0	29.1±0.2	29.8±1.4
NM-7	granodiorite	4250	91° 53.6'	29° 15.4'	Ksp	0.005419[a]	27.7	-	-
NM-7	granodiorite	4250	-	-	Bio	0.005419[a]	27.6	27.6±0.2	27.8±1.2
YANS-1	granodiorite	4760	92° 11.5'	29° 18.8'	Ksp	0.005343[a]	24.0	-	-
YANS-1	granodiorite	4760	-	-	Bio	0.005344[a]	25.7	25.8±0.4	26.1±1.4
YANS-2	granodiorite	4640	92° 11.2'	29° 18.5'	Bio	0.005349[a]	24.6	24.7±0.6	24.1±2.6
YANS-3	granodiorite	4520	92° 10.7'	29° 18.2'	Bio	0.005353[a]	24.1	24.2±0.4	25.1±1.2
YANS-4	granodiorite	4300	92° 9.8'	29° 17.9'	Bio	0.005359[a]	23.3	23.3±0.6	25.7±2.2
YANS-5	granodiorite	4200	92° 9.4'	29° 18.0'	Bio	0.005369[a]	26.4	26.5±0.4	27.3±0.6
YANS-6	granodiorite	4000	92° 9.2	29° 17.7'	Ksp	0.005372[a]	25.0	-	-
YANS-6	granodiorite	4000	-	-	Bio	0.005375[a]	26.0	26.0±0.2	26.0±0.8
YANS-8	granodiorite	3800	92° 9.0'	29° 17.6'	Bio	0.005386[a]	26.2	26.2±0.2	25.9±4.2
YANS-9	granodiorite	3720	92° 8.9	29° 17.4'	Bio	0.005394[a]	26.4	26.5±0.2	25.8±2.4
YANS-10	granodiorite	3640	92° 8.8'	29° 17.4'	Bio	0.005399[a]	24.3	24.5±0.8	28.6±2.4
YANS-11	granodiorite	3560	92° 8.7'	29° 17.3'	Ksp	0.005402[a]	23.1	-	-
YANS-11	granodiorite	3560	-	-	Bio	0.005404[a]	26.0	26.0±0.4	27.5±4.7
ZH-1-94	granodiorite	3606	91° 52.8'	29° 15.9'	Ksp	0.005455[c]	27.1	-	-
ZH-1-94	granodiorite	3606	-	-	Bio	0.005448[c]	27.8	27.8±0.2	27.4±1.2
ZH-1-94	granodiorite	3606	-	-	Hbd	0.005630[c]		30.5±1.0	33.0±2.0
ZH-9A-94	granodiorite	3750	92° 10.1'	29° 17.6'	Ksp	0.005441[c]	30.0	-	-
ZH-11-94	granodiorite	3500	92° 9.9'	29° 17.4'	Ksp	0.005433[c]	28.3	-	-
ZH-11-94	granodiorite	3500	-	-	Bio	0.005424[c]	26.5	26.5±0.2	25.3±1.2
N-5	granodiorite	3680	92° 6.4'	29° 17.3'	Ksp	0.005268[a]	29.3	-	-
N-5	granodiorite	3680	-	-	Hbd	0.005702[c]	64.0	64±6	61±8
N-6	diorite	3550	92° 13.0'	29° 15.3'	Ksp	0.005274[a]	45.9	-	-
N-6	diorite	3550		-	Bio	0.005276[a]	64.5	64.4±1.4	64.2±3.0
N-6	diorite	3550	-	-	Hbd	0.006636[b]	67.0	68±8	64±22
N-7	orthogneiss	3550	92° 13.0'	29° 15.3'	Hbd	0.005703[c]	62.6	64.4±1.6	63.7±3.2
N-8	granodiorite	3840	92° 13.3'	29° 19.8'	Ksp	0.005280[a]	21.0	-	-
N-8	granodiorite	3840	-	-	Bio	0.005282[a]	22.5	22.7±0.2	23.0±0.2
N-8	granodiorite	3840	-	-	Hbd	0.006637[b]	32.7	30.8±1.0	30.9±1.6
N-9	granodiorite	3840	92° 13.3'	29° 19.8'	Ksp	0.005286[a]	18.5	-	-
N-9	granodiorite	3840	-	-	Hbd	0.005704[c]	28.8	30.5±0.4	29.2±1.8
N-10	granodiorite	3750	92° 13.4'	29° 19.3	Ksp	0.005291[a]	26.7	-	-
N-10	granodiorite	3750	-	-	Bio	0.005293[a]	25.6	25.6±0.2	25.0±0.8
N-11	granodiorite	3750	92° 13.4'	29° 19.3'	Ksp	0.005296[a]	22.6	-	-
N-11	granodiorite	3750	-	-	Bio	0.005298[a]	23.4	23.7±0.8	24.8±1.6
N-11	granodiorite	3750	-	-	Hbd	0.005704[c]	34.2	38±2	37±6
N-12	granodiorite	3680	92° 13.5'	29° 17.8'	Ksp	0.005301[a]	22.4	-	-
N-12	granodiorite	3680	-	-	Bio	0.005303[a]	28.9	29.0±0.2	29.2±0.8
N-13	granodiorite	3720	92° 14.8'	29° 16.4'	Ksp	0.005306[a]	26.2	-	-
N-13	granodiorite	3720	-	-	Bio	0.005307[a]	33.1	33.1±0.6	31±4
N-13	granodiorite	3720	-	-	Hbd	0.005702[c]	40.6	44±4	44±4
N-14	granodiorite	3460	92° 12.5	29° 15.6'	Ksp	0.005311[a]	30.2	-	-
N-14	granodiorite	3460	-	-	Bio	0.005313[a]	25.7	25.7±0.4	26.8±0.4
N-16	granite	3460	92° 11.1'	29° 17.0'	Ksp	0.005317[a]	23.8	-	-
N-16	granite	3460	-	-	Mus	0.005318[a]	39.2	39.2±0.4	37.2±4.8
N-17	granodiorite	3560	92° 9.3'	29° 17.3'	Bio	0.005321[a]	27.7	27.6±0.4	26.6±3.0
N-19	syenite	3600	92° 0.6'	29° 14.4'	Ksp	0.005327[a]	23.5	-	-
N-19	syenite	-	-	-	Hbd	0.005700[c]	61.6	77±16	83±14
N-21	granodiorite	3880	91° 47.5	29° 15.6'	Ksp	0.005324[a]	47.9	-	-
N-21	granodiorite	3880	-	-	Bio	0.005325[a]	52.5	52.6±1.4	
N-21	granodiorite	3880	-	-	Hbd	0.005698[c]		63±3	
N-25	granodiorite	3900	92° 4.8	29° 18.4'	Ksp	0.005326[a]	34.5	-	-
N-25	granodiorite	3900	-	-	Hbd	0.005695[c]		66.6±0.5	

[a]Irradiation UM75, 70 hours in location H-75; $(^{40}Ar/^{39}Ar)_K = 0.031$; $(^{38}Ar/^{39}Ar)_K = 0.012$; $(^{36}Ar/^{37}Ar)_{Ca} = 2.5 \times 10^{-4}$; $(^{39}Ar/^{37}Ar)_{Ca} = 7.3 \times 10^{-4}$.
[b]Irradiation UM79, 45 hours in location L-67; $(^{40}Ar/^{39}Ar)_K = 0.031$; $(^{38}Ar/^{39}Ar)_K = 0.012$; $(^{36}Ar/^{37}Ar)_{Ca} = 2.5 \times 10^{-4}$; $(^{39}Ar/^{37}Ar)_{Ca} = 7.3 \times 10^{-4}$.
[c]Irradiation UM82, 100 hours in location H-75; $(^{40}Ar/^{39}Ar)_K = 0.037$; $(^{38}Ar/^{39}Ar)_K = 0.013$; $(^{36}Ar/^{37}Ar)_{Ca} = 3.1 \times 10^{-4}$; $(^{39}Ar/^{37}Ar)_{Ca} = 7.3 \times 10^{-4}$.
Minerals are K-feldspar, Ksp; biotite, Bio; hornblende, Hbl; muscovite, Mus.

TABLE 2. Major and Trace Element Concentrations of Granitoid Samples From the Zedong Region

					Sample						
	NM-1	NM-2	NM-3	NM-4	NM-5	NM-6	NM-7	ZH-3-92	ZH-1-94	YANS-2	YANS-4
SiO_2	66.0	69.5	70.1	60.8	65.9	66.2	65.8	71.1	66.8	71.5	71.3
Al_2O_3	16.0	15.2	15.1	17.4	16.1	15.8	15.5	14.6	15.6	15.3	15.1
Fe_2O_3	3.73	1.43	2.72	5.17	3.54	3.63	3.67	2.06	3.36	1.84	2.26
MnO	0.07	0.04	0.05	0.09	0.06	0.06	0.07	0.04	0.06	0.04	0.06
MgO	2.08	1.07	0.95	2.8	1.75	1.76	2.05	0.9	1.74	0.55	0.69
CaO	3.82	3.68	3.08	5.43	3.87	3.84	3.44	2.66	3.87	1.77	1.86
Na_2O	4.09	3.81	4.38	4.52	4.2	4.27	3.7	3.84	4.26	3.76	3.7
K_2O	3.34	4.45	2.65	2.55	3.42	3.1	4.64	4.02	3.24	4.77	4.55
TiO_2	0.50	0.357	0.35	0.6	0.44	0.458	0.446	0.315	0.432	0.232	0.334
P_2O_5	0.22	0.18	0.17	0.34	0.25	0.27	0.32	0.15	0.26	0.1	0.11
LOI	0.71	0.72	0.7	0.95	0.58	0.55	0.56	0.7	0.46	0.82	0.63
Total	100.6	100.5	100.2	100.7	100.1	100.0	100.2	100.4	100.1	100.7	100.5
V	85	46	53	117	75	75	74	45	75	27	35
Cr	27	38	nd	41	35	34	59	27	47	nd	nd
Co	36	20	27	39	24	27	54	38	32	27	16
Ni	27	51	33	40	30	30	47	29	31	nd	nd
Cu	16	26	10	48	nd	nd	31	32	49	nd	nd
Zn	60	40	41	90	49	53	55	51	69	47	47
Ga	20	19	20	22	19	20	19	19	21	19	19
Rb	128	174	118	105	113	121	192	170	134	205	219
Sr	997	635	645	1160	926	882	743	605	869	399	379
Y	11	9	9	13	11	11	11	10	11	9	16
Zr	134	166	137	148	143	177	183	158	152	161	179
Nb	9	12	16	10	10	10	9	14	12	7	12
Cs	7.7	5.7	6.9	11.5	6.3	5.8	8.1	6.4	5.4	8.1	12.4
Ba	1280	672	293	1110	1180	835	1230	664	879	741	617
La	42.4	38.6	50.3	42.6	51.2	57.6	58.2	37.2	59.1	40.0	38.1
Ce	82.4	77.8	89.1	88.3	100	106	101	73.7	108	69.5	80.9
Pr	8.65	7.77	8.36	9.33	10.2	10.5	9.97	7.55	10.6	6.41	9.00
Nd	30.3	26.5	27.8	34.5	35.5	36.7	35.1	26.0	36.7	20.7	31.9
Sm	4.7	3.9	3.9	5.5	5.1	5.4	5.1	3.8	5.3	3.0	5.4
Eu	1.29	0.97	1.03	1.59	1.40	1.37	1.17	0.97	1.39	0.72	1.09
Gd	3.3	2.6	2.7	4.0	3.6	3.6	3.6	2.8	3.7	2.1	3.8
Tb	0.4	0.3	0.3	0.5	0.4	0.4	0.4	0.3	0.4	0.3	0.5
Dy	2.0	1.6	1.6	2.5	2.0	2.0	2.1	1.6	2.1	1.4	2.8
Ho	0.4	0.3	0.3	0.4	0.4	0.4	0.4	0.3	0.4	0.3	0.5
Er	1.0	0.8	0.8	1.2	1.0	1.0	1.0	0.9	1.0	0.8	1.5
Tm	0.13	0.12	0.12	0.17	0.12	0.13	0.13	0.12	0.14	0.13	0.21
Yb	0.9	0.8	0.8	1.0	0.9	0.9	0.9	0.9	0.9	0.9	1.4
Lu	0.13	0.13	0.14	0.16	0.14	0.13	0.14	0.13	0.13	0.14	0.21
Hf	4.2	5.1	4.4	4.5	4.3	5.6	5.7	5.0	4.7	5.3	6.0
Ta	1.2	1.4	1.7	1.2	1.1	1.2	1.4	2.0	1.5	1.1	1.6
W	194	128	179	171	114	147	335	234	177	186	101
Tl	0.7	0.8	0.6	0.7	0.6	0.7	0.9	0.9	0.7	1.2	1.2
Pb	27	15	19	31	21	28	27	33	24	37	31
Th	19.2	25.9	32.6	13.7	32.4	26.1	28.1	31.7	32.0	30.6	36.1
U	3.0	7.1	7.8	5.5	3.7	3.7	5.9	9.2	8.1	5.5	4.8

Major element concentrations in wt. %, and trace element concentrations in ppm.

Jarrell-Ash ENVIRO II inductively coupled spectrometer and for trace elements using a Perkin Elmer SCIEX ELAN 6000 inductively coupled plasma mass spectrometer. Results are given in Table 2 (oxides in %; trace elements in ppm).

3.5. Numerical Modeling

The counterposed thrust systems in the Zedong region present several challenges in interpreting the thermal history results obtained from isotopic techniques. The first is that the functional form of the thermal evolution experienced by a geochronological system has a first-order effect on the nature and quality of the temperature history information that is possible to recover from a thermochronometer. If, for example, the isotopic system closed during monotonic cooling, such as might be expected in the hanging wall of a thrust fault, then an unique thermal history can be obtained [see *McDougall and Harrison*, 1999]. Conversely, a temperature history involving reheating, such as that experienced in the footwall of a thrust due to tectonic burial, shear heating, sedimentation, or some combination of these factors, can only yield broad temperature-time constraints [e.g., *Quidelleur et al.*, 1997]. Thus before we can use thermochronological data to constrain tectonic rates, we must first broadly anticipate the form of the history involved. Our second significant challenge is to identify, and potentially isolate, thermal effects produced by the two episodes of thrusting. Finally, we must constrain a thermal model with a thrust geometry and mode of heat flow consistent with independent geologic relationships in order to extract quantitative tectonic information from the thermochronological results.

We have simulated the thermal evolution of the central portion of the Zedong Window using a two-dimensional, finite difference model that employs alternating-direction implicit techniques to describe thrusting along a fault with a ramp-flat geometry and 1-km-thick shear zone. We assume a ramp dip (ϕ) of 15°, consistent with observed geologic relationships, with a horizontal portion of the thrust at a depth of 14 km. Thus the uplift rate U above the ramp is given by $V \sin \phi$, where V is the slip rate. As previously stated, we interpret the presently observed dip of the GT of 30°-75° to reflect post slip steepening due to activity on the RZTS. The numerical model is a variant of that used in earlier investigations and the basic elements of the calculations are described elsewhere [*Harrison et al.*, 1997a, b, 1998; *Quidelleur et al.*, 1997]. In the present case, we utilized a calculation region of 300 km horizontal (x) by 40 km vertical (z) with a resolution of 900 x 450 grid points. Boundary conditions include a constant basal heat flux and zero lateral heat flux. The region to be compared with the isotopic results was positioned sufficiently far from the sides and base of the numerical grid such that the boundary conditions employed should have negligible effects on the temperature history results. Thermal effects of topography were simulated by varying surface temperature equal to the product of the change in elevation and the geothermal gradient. The initial geotherm was calculated [*Turcotte and Schubert*, 1982, equation 4-31] using the following parameters: thermal diffusivity, $\kappa = 10^{-6}$ m^2/s; initial surface flux, $Q_S = 85$ mW/m^2; basal heat flux, $Q_B = 30$ mW/m^2; and radioactivity scale length, $z^* = 15$ km. This geotherm is reasonably well approximated by a linear fit over the upper 10 km corresponding to ~30°C/km. This value is typical of an active arc setting [e.g., *Henry and Pollack*, 1988] and within uncertainty of the value estimated for the Quxu region at circa 30 Ma [see *Copeland et al.*, 1995] (Plate 1). Frictional

heating corresponding to a shear stress (σ) of 20 MPa was added within the shear zone [see *Harrison et al.*, 1998].

4. Results

4.1. U-Pb Zircon Crystallization Ages

A total of 53 U-Pb spot analyses were undertaken on zircons separated from three samples (NM-1, NM-7, and ZH-1-94) of the Yaja granodiorite, 13 analyses on two samples (YANS-5 and YANS-10) of the Kangagang granodiorite, and 9 analyses of zircons from sample N-9. These zircons are characterized by radiogenic ^{206}Pb contents (assuming a common ^{206}Pb/^{204}Pb of ~19) that vary from 25 to 99%. Results from N-9 are highly radiogenic and thus insensitive to assumptions regarding the composition of common Pb (Table 2). The nine measurements plot within uncertainty of concordia and yield a weighted mean ^{206}Pb/^{238}U age of 48.9±0.8 Ma (2σ) (Mean Square of Weighted Deviates (MSWD) = 0.89), which we interpret to be the age of crystallization.

Analyses with lower radiogenic yields have large associated errors in calculated model ages due to uncertainties in the correction for common Pb. However, provided that grains have concordant U-Pb systems, a good assumption given their youth and relatively low U contents (typically 100-800 ppm), the necessity of assuming a composition of common Pb can be circumvented. Specifically, data uncorrected for common Pb should define a line which intersects concordia at the age of crystallization and has a slope corresponding to the common ^{206}Pb/^{207}Pb ratio [*Dalrymple et al.*, 1999]. Such a relationship appears to be borne out by both the Yaja and Kangagang granodiorites (Figure 1).

With one exception, all of the zircon grains from the Yaja granodiorite yield model ^{206}Pb/^{238}U ages of approximately 30 Ma. The lone exception, presumably an inherited grain, yields a concordant age of 73±3 Ma. The clustering of Oligocene ages from samples obtained from a single mapable unit suggests that all three samples are members of the same age population and share a common Pb isotopic composition. A plot of the uncorrected results on concordia yields the expected linear relationship with an age of 30.42±0.42 Ma (2σ) and an MSWD of 1.1 (Figure 1a). The slope of the aggregated data corresponds to an initial ^{207}Pb/^{206}Pb ratio of 0.79±0.04 (2σ), consistent with modern terrestrial Pb and anthropogenic sources [*Faure*, 1986].

The nine spot U-Pb measurements of zircons from sample YANS-10 together with the four from sample YANS-5 (Figure 1b) yield an age of 42.5±1.0 Ma (2σ) and an MSWD of 0.92, interpreted to be the crystallization age of the Kangagang granodiorite. The common ^{207}Pb/^{206}Pb ratio of 0.80±0.10 (2σ) is also similar to modern Pb and is indistinguishable from the Yaja result.

4.2. Granitoid Geochemistry

Previous major and trace element geochemistry of the Gangdese batholith [*Debon et al.*, 1986; *Coulon et al.*, 1986; *Miller et al.*, 1999] indicate that this composite batholith is somewhat uncharacteristic of typical convergent margin magmatism. The Gangdese batholith is high-K calc-alkaline, or monzonitic [*Debon et al.*, 1986]. The major and trace element compositions of the Yaja and Kangagang granodiorites
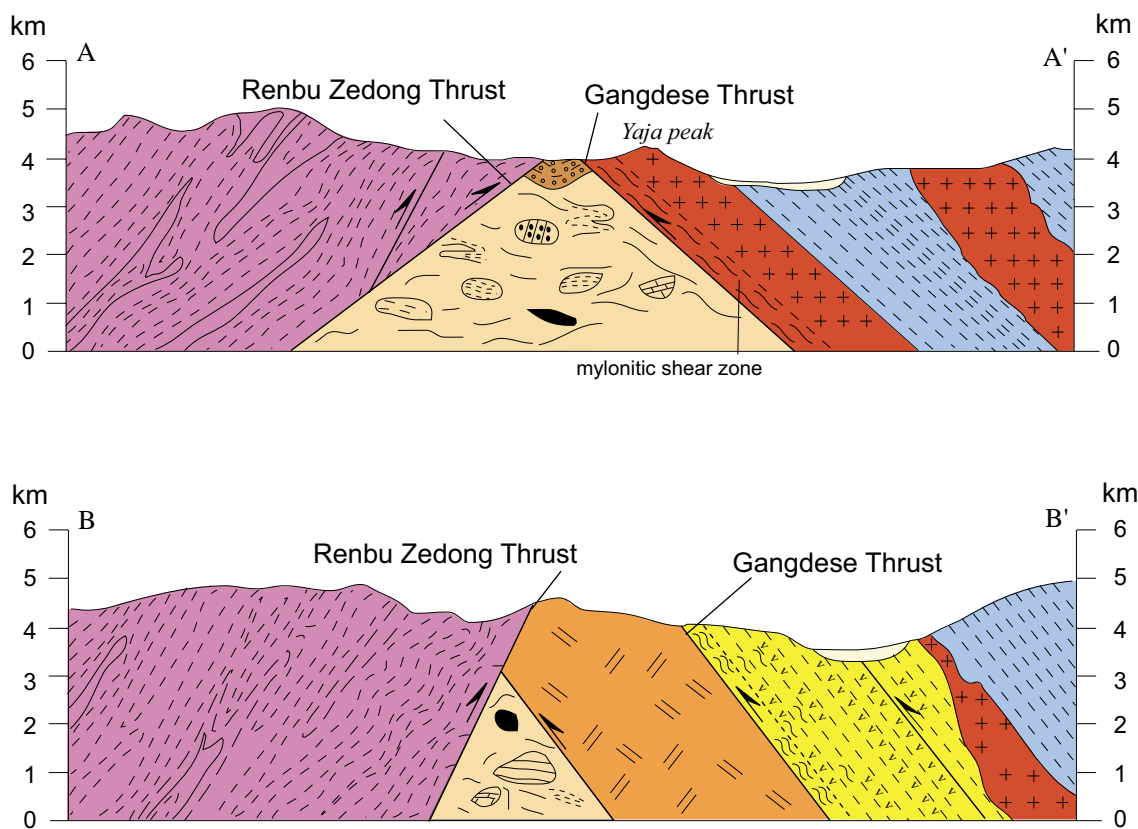
Plate 3. Geologic cross sections for the Zedong area (see Plate 2 for locations of sections A-A' and B-B'). Note that the Gangdese Thrust, its hanging wall bedding, and tabular granitoid bodies are subparallel.
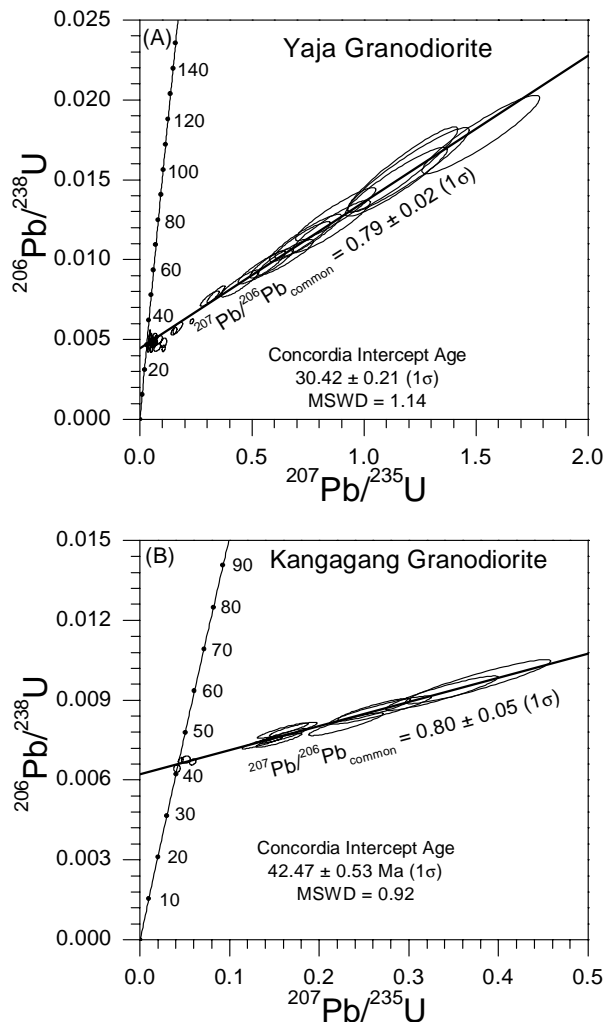
study (Table 1), we first focus on the 13 hornblende and 27 biotite results. The instability of these phase during in vacuo heating prompts us to interpret results obtained from them in terms of bulk closure ages rather than with a diffusion model [see *McDougall and Harrison*, 1999]. A summary of the total fusion, weighted mean, and inverse isochron model ages calculated for each of the samples appears in Table 1. Note that the indicated ±2σ uncertainties have been scaled by a factor equal to the square root of the MSWD to ensure that they reflect the age variability exhibited by a given sample. Given the sensitivity of total fusion ages to excess ^{40}Ar contributed by relatively small, unradiogenic gas release increments and the difficulties of interpreting isochrons from unradiogenic samples that fail to exhibit adequately defined linear arrays, we accept the weighted mean ages as best representing the time of bulk closure. Temperatures corresponding to the time of hornblende and biotite bulk closure are estimated from diffusion parameters summarized by *McDougall and Harrison* [1999]. A single ^{40}Ar/^{39}Ar muscovite age was obtained from sample N-16, a two-mica granite.

4.3.2. K-feldspar. We have calculated thermal histories from ^{40}Ar/^{39}Ar results for K-feldspars using the multidiffusion domain model (MDD) [*Lovera et al.*, 1989]. As an example, results from sample NM-1 are shown in Figure 3. Details of the methods used to calculate kinetic parameters and thermal histories are described in detail by *Lovera et al.* [1997]. In the case of monotonic cooling, a unique *T-t* history can be obtained [*Lovera et al.*, 1997; *McDougall and Harrison*, 1999]. However, if the sample did not cool monotonically (for example, it was reheated due to burial by the upper plate of the RZT), then a unique solution is not possible. Even so, the maximum temperatures that could have obtained given geologically reasonable heating rates may be determined. Inferences may also be made regarding the probability that a sample experienced specific temperatures at given times. To accomplish this, the MDD model can be generalized to samples that have experienced combinations of slow cooling and reheating. We use a variational approach [*Quidelleur et al.*, 1997] in which an initial arbitrary thermal history is itera-
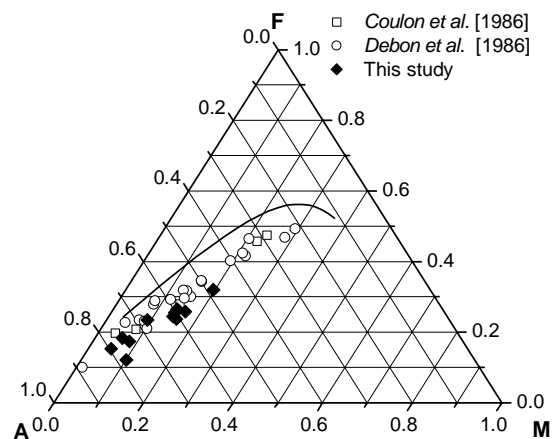
Figure 1. (a) U-Pb concordia plot for the Yaja granodiorite. When plotted uncorrected for common Pb, 43 of 44 U-Pb ion microprobe spot analyses on zircons from samples NM-1, NM-7, and ZH-1-94 yield a linear relationship on a concordia plot with an age of 30.42±0.42 Ma (2σ) and initial ^{207}Pb/^{206}Pb ratio of 0.79±0.04 (2σ). A single inherited grain with an age of 73 Ma was also found. (b) Thirteen U-Pb ion microprobe spot analyses on zircons from samples YANS-5 and YANS-10 from the Kangagang granodiorite yield an age of 42.5±1.0 Ma (2σ) and common ^{207}Pb/^{206}Pb ratio of 0.80±0.10 (2σ).

(Table 2 and Figure 2) strongly resemble previous results from the Gangdese batholith. For example, they overlap the calc-alkaline trend defined by samples from the Quxu and Dazhuka regions [*Debon et al.*, 1986]. We can therefore assume that the processes responsible for genesis of the precollisional (i.e., before 55 Ma) batholith are broadly similar to those that produced melting later when collision was well underway.

4.3. ^{40}Ar/^{39}Ar Measurements

4.3.1. Hornblende and biotite. In presenting the large number of ^{40}Ar/^{39}Ar measurements obtained in the present

Figure 2. AFM diagram showing results from Yaja and Kangagang granodiorites (this study) in comparison with earlier geochemical results from igneous rocks of the Gangdese batholith at Maquiang [*Coulon et al.*, 1986], Dazhuka, and Quxu [*Debon et al.*, 1986].
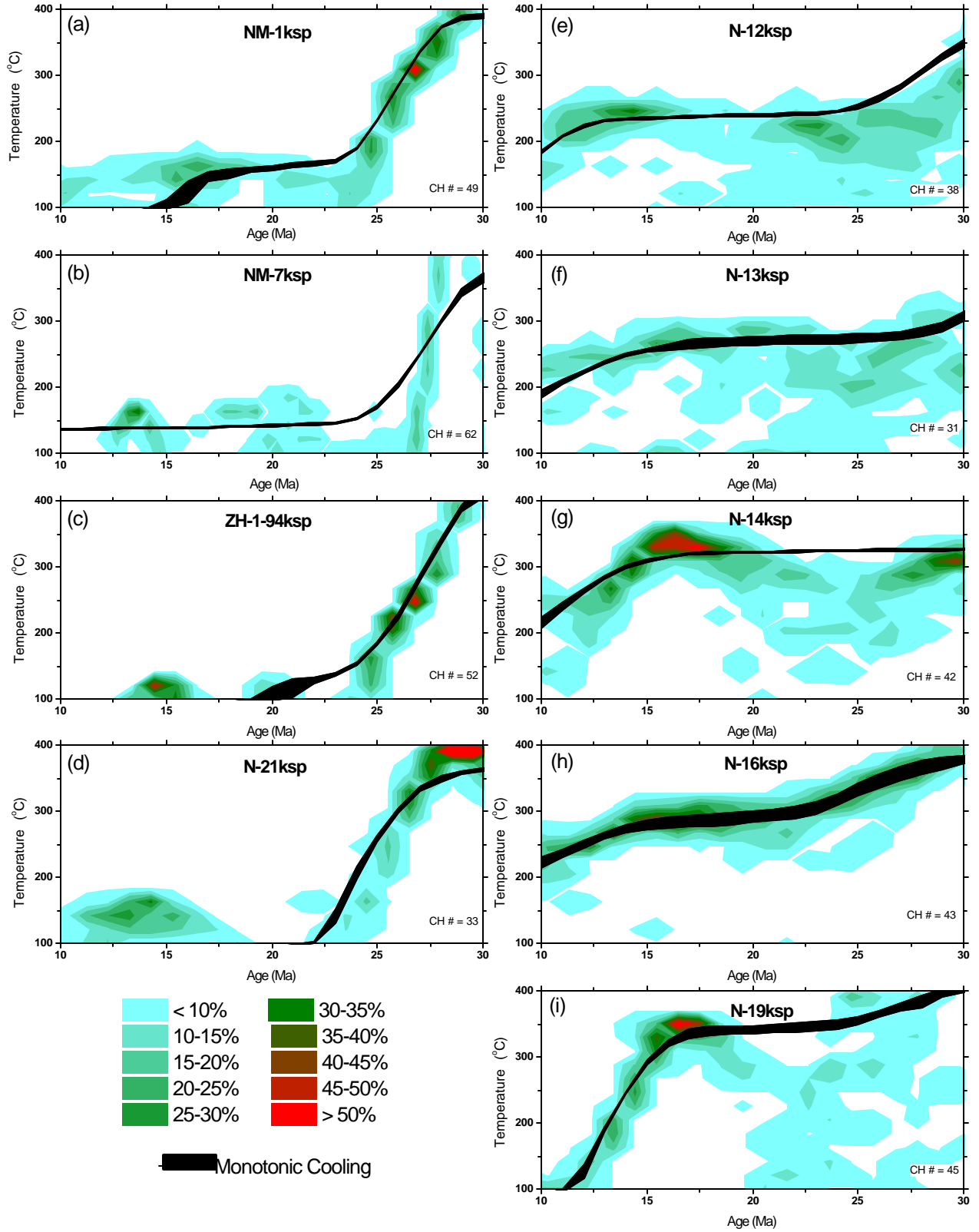
Plate 4. Thermal histories derived from MDD modeling of K-feldspar ^{40}Ar/^{39}Ar age spectra. The solid curve shows thermal history results calculated assuming monotonic cooling. Also shown are contours of thermal histories that allow for reheating that provide a degree of agreement to the age spectrum such as $|\chi^2|/\chi^2_{min} < 0.5$. The colored contours (see legend) indicate the percentage of temperature-time histories which pass through 30°C by 0.4 Ma elements of T-t space. CH# is number of cooling histories that satisfied the minimization criteria for the age spectrum out of 80-90 runs.
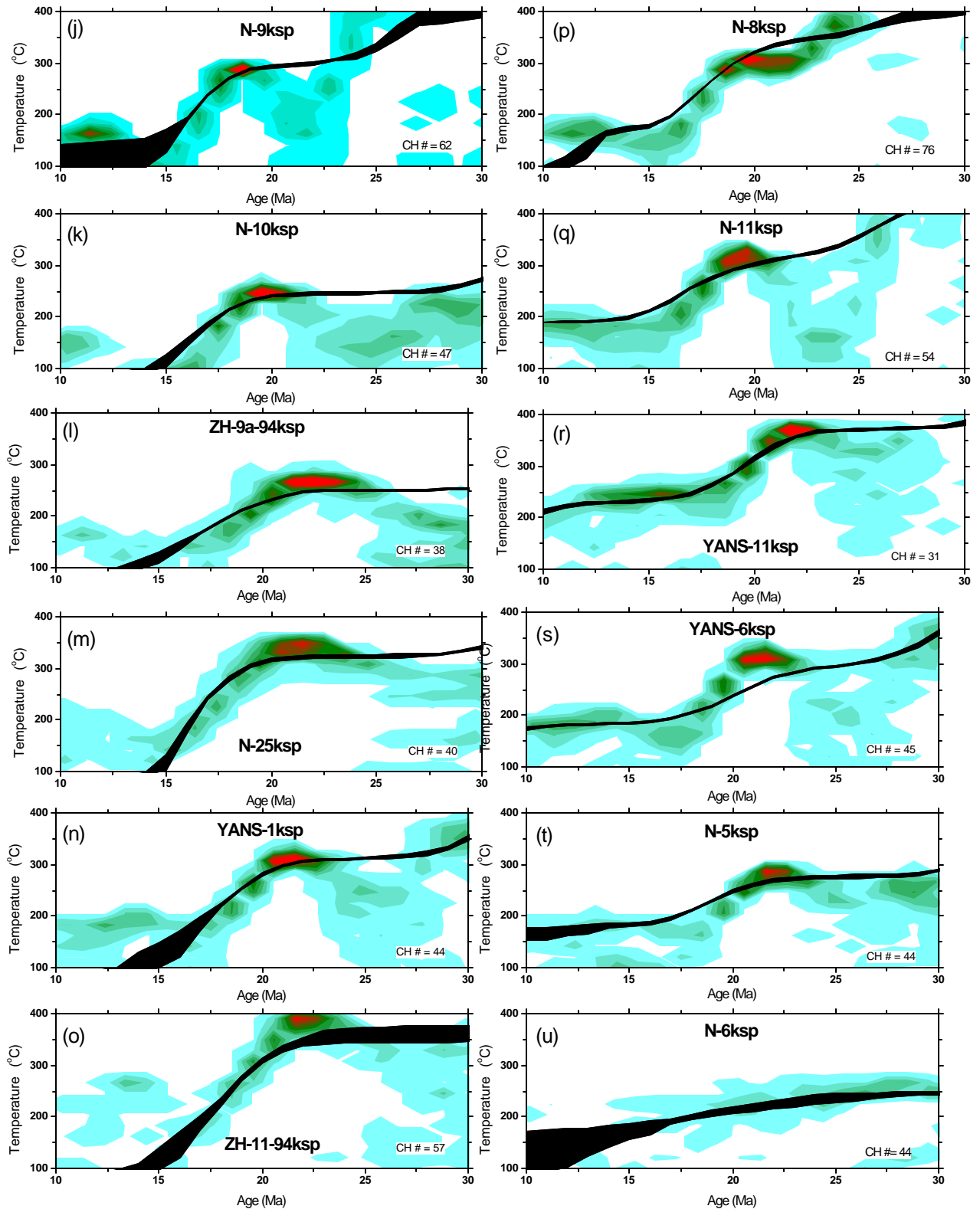
Plate 4. (continued)
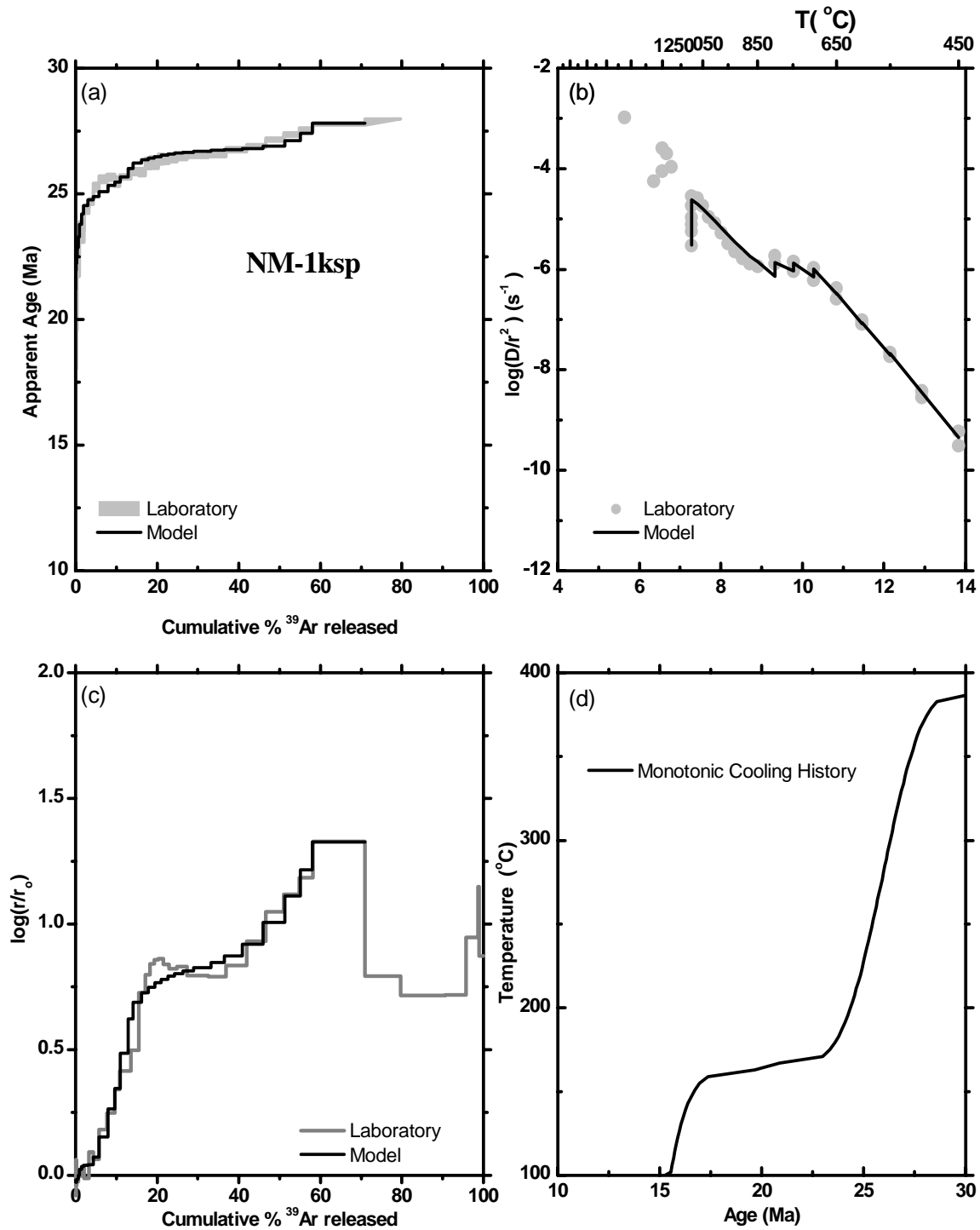
Figure 3. Thermal history results from NM-1 K-feldspar. (a) The measured age spectrum and model fits produced by best fit thermal histories; (b) the measured and model diffusion values calculated from ^{39}Ar diffusivities and the MDD model, respectively; (c) the $\log(r/r_o)$ plot; and (d) the calculated thermal history assuming monotonic cooling.

tively varied until an optimal statistical fit to the age spectrum is obtained. Repetition of this process potentially allows exploration of the full range of thermal history solutions capable of satisfying the measured age spectrum. Because the clarity of the thermal history information derived in this way is diminished relative to that obtained assuming monotonic cooling, we combine all results to construct contour plots which indicate the probability of attaining specific T-t conditions (Plate 4). Together with closure ages estimated from the hydrous phases, the K-feldspar derived thermal histories provide the basis for reconstructing the thermal history of the region (Plate 5).

5. Discussion

5.1. Geochronology of the Footwall of the Gangdese and Renbu Zedong Thrusts

Our interpretation of the geochronology of the rocks exposed in the footwalls of the Gangdese and Renbu Zedong Thrusts is limited by poor exposure due to alluvium of the Yalu Tsangpo (Plate 2). The local Cretaceous fossil age provides an upper bound on the timing of melange assembly. The melange is overlain by a conglomerate unit that contains Oligocene fossils but may be as young as Miocene [*Yu and Zheng*, 1979]. Plutonic bodies sampled in the footwall generally appear to be slivers of the hanging wall thrust over the melange and possibly represent an early phase of the Gangdese Thrust. The Tertiary conglomerate was deposited unconformably on top of both melange and plutonic sheets [*Yin et al.*, 1999].

We obtained $^{40}Ar/^{39}Ar$ data on four samples from what we interpret to be thrust sheets in the footwall of the opposing thrusts. The four samples, diorite (N-6), orthogneiss (N-7), syenite (N-19), and granodiorite (N-21), share several common features in their geochronology. For example, all four yield $^{40}Ar/^{39}Ar$ hornblende ages in the range 67 to 62 Ma. The concordance of hornblende and biotite ages from sample N-6 at ~67 Ma suggests this was a time of rapid cooling following metamorphic recrystallization. This concordance also limits the peak temperature experienced by this rock subsequent to emplacement to <350°C [*McDougall and Harrison*, 1999]. Individual steps in the K-feldspar age spectrum are as old as 61 Ma and decrease in a systematic fashion to ages as young as 13 Ma. The adjacent orthogneiss sample N-7 yields a hornblende $^{40}Ar/^{39}Ar$ age of 64.4±0.8 Ma. Although low radiogenic yields were obtained for the $^{40}Ar/^{39}Ar$ step heating analyses of hornblende from syenite sample N-19, the age is clearly pre-Tertiary. However, the K-feldspar age spectrum obtained from this sample indicates temperatures >350°C were maintained prior to 30 Ma and above ~150°C until about 12 Ma. In contrast, the K-feldspar from granodiorite sample N-21 (Table 1 and Plate 2) was effectively closed to argon loss at 25 Ma and preserves ages as old as 45 Ma. In this regard, it bears striking similarity with the samples from the Yaja traverse (i.e., NM1-7, ZH-1-94). Given the general concordance of hornblende $^{40}Ar/^{39}Ar$ and U-Pb zircon ages in Gangdese plutons [e.g., *Copeland et al.*, 1995], we infer an emplacement age for N-21 of about 63 Ma. Similar intrusion ages are found elsewhere in the batholith [e.g., *Schärer et al.*, 1984; *Quidelleur et al.*, 1997].

The emplacement of the granitoid thrust sheets in the GT footwall must postdate formation of the melange and predate deposition of the Tertiary conglomerate. Ages derived from fossils in the two units [*Yu and Zheng*, 1979] provide only weak constraints on the timing of this activity (i.e., between Late Cretaceous and Miocene). The thermal histories obtained from $^{40}Ar/^{39}Ar$ analyses of the three footwall K-feldspars (i.e., N-6, N-19, and N-21) suggests elevated temperature prevailed during the early Miocene, but N-21 bears a sufficient similarity to results from the Yaja traverse to suggest that it may represent a sliver from the GT hanging wall. The magnitude of slip between the granitoid thrust sheets in the GT footwall and the melange is difficult to quantify, but the low metamorphic grade of the melange [*Yin et al.*, 1999] and low (<350°C) post-Cretaceous temperatures documented by thermochronometry of samples from all granitoid thrust sheets except that of N-19 suggest relatively little displacement.

5.2. Recognition of Distinct Thermal History Domains Within the Hanging Wall of the Gangdese Thrust

Our thermal history results allow us to define three distinct regions within the GT hanging wall. The first, region I in Plate 2, is represented by results from the NM traverse and, possibly, sample N-21. K-feldspars from this region were effectively closed to Ar loss by ~23 Ma. In contrast, thermochronometric results from the eastern portion of the Zedong Window (regions II and III in Plate 2) were obtained from positions much closer to where the Renbu Zedong Thrust reoccupies the suture zone (Plate 1). Samples from both domains indicate a more protracted thermal history to that seen in region I, with minimum ages in K-feldspar $^{40}Ar/^{39}Ar$ age spectra of about 10 Ma (e.g., N-13 and N-14). We interpret the later argon degassing in the eastern portion of the Zedong Window relative to that in the vicinity of the Yaja pluton as resulting from a combination of factors that include (1) exposure of a deeper structural level, (2) persistence of greater topography, (3) a greater thickness of the RZT hanging wall, and (4) folding of GT hanging wall rocks produced by motion of the RZT (Plate 2).

The change in cooling style between the central (region I) and eastern (regions II and III) portions of the Zedong Window appears to have greater regional significance. Thermochronological results along strike from Yaja to as far west as Quxu (Plate 1) are characterized by late Oligocene-early Miocene rapid cooling [*Copeland et al.*, 1987, 1995; *Pan et al.*, 1993, this study], which can be ascribed either directly to slip on the GT or due to denudation following crustal thickening via the GT. In contrast, thermochronological results east of Yaja to Lang Xian (Plate 1) indicate rapid cooling during the middle to late Miocene [*Quidelleur et al.*, 1997; this study]. Near Lang Xian (Plate 1), a suite of samples collected in the footwall of the RZT shows evidence of a significant thermal disturbance related to displacement along the RZT [*Quidelleur et al.*, 1997]. In particular, $^{40}Ar/^{39}Ar$ ages of biotite and K-feldspar increase systematically away from the trace of the RZT, from about 60 Ma in the north to about 10 Ma in the south near the fault. Detailed analysis of K-feldspar age spectra and a thermal model of the effect of the emplacement history of the nappe suggest that the RZT was active between 18 and 10 Ma. In the following discussion we constrain the slip history of the GT using results from region I. We later consider results from regions II and III to estimate the magnitude of thermal overprinting due to activity along the RZT.

5.3. Slip Along the Gangdese Thrust

In general, dating geologic features that cut across or are cut by faults provides only lower and upper bounds, respectively, on the timing of slip and thus can only constrain a minimum estimate of slip rate. Alternatively, the rate of cooling inferred from the closure of isotopic systems can be related to the rate of displacement along a fault, but only in cases in which a significant temperature contrast developed across the fault [e.g., *Harrison et al.*, 1995]. For example, although cooling produced by motion along a fault ramp can in principle constrain the rate of slip (i.e., the more rapid the

cooling, the faster the slip rate), little temperature contrast is produced by motion along a shallowly inclined decollement in the presence of horizontal isotherms. However, our crystallization age for the Yaja granodiorite combined with thermochronological results from other region I samples from the central portion of the Zedong Window potentially provide both kinds of information from which we are able to place model-based constraints on the timing and evolution of the Gangdese Thrust.

5.3.1. Emplacement of the Yaja granodiorite. A constraint on the timing of slip along the present trace of the Gangdese Thrust is obtained from the crystallization age of the Yaja granodiorite, situated within and immediately above the ductile shear zone which exhibits similar mylonitic fabrics to other hanging wall lithologies adjacent the GT. We interpret the U-Pb ion microprobe zircon date of 30.4±0.4 Ma as the emplacement age of the Yaja granodiorite and thus conclude that the ductile shear zone must have been active during or subsequent to this time.

A ~4-km-diameter spherical pluton is expected to cool by conduction to near ambient conditions within 1 million years [*Crank*, 1975, p. 30]; a sill-like geometry would cool even quicker. All eight biotite and K-feldspar samples from the Yaja granodiorite yield total gas $^{40}Ar/^{39}Ar$ ages between 29.3 and 27.0 Ma, indicating that these isotopic systems were open to argon loss subsequent to emplacement. From knowledge of the argon degassing kinetics of both phases (see Figure 3 and *McDougall and Harrison* [1999]), we thus infer that the ambient temperature of the Yaja granodiorite was >350°C. Because the hornblendes yield an average $^{40}Ar/^{39}Ar$ age of 32.0±1.2 Ma (Table 1), indistinguishable at 2σ from the U-Pb zircon age (Figure 1a), the ambient temperature cannot have exceeded 450°C. Thus we estimate the temperature at the present level of exposure prior to intrusion was 400±50°C. For an initial geotherm of 30°C/km (see section 3.5) the estimated ambient temperature corresponds to an emplacement depth for ZH-1-94 of ~13 km.

Two lines of evidence suggest that the GT became active only after emplacement of the Yaja granodiorite. The first is the equant shape and undeformed nature of the pluton (Plate 2) immediately outside the shear zone, which suggests that emplacement occurred in the absence of high deviatoric stress and thus prior to fault activity. The relatively high temperature fabrics within the sheared granodiorite (≥450°C), however, suggest that the fault was active during the first million years following intrusion when sufficient magmatic heat was still retained.

The second line of evidence is the age of the Kailas-type conglomerate (Plate 1), which is composed largely of Gangdese plutonic and volcanic cobbles and thought to represent debris accumulated to the south of the denuding batholith [*Gansser*, 1964]. While paleobotanical age assessment (late Eocene to Miocene?) of this widespread unit is problematic [*Gansser*, 1964], thermochronological results indicate a late Oligocene upper limit for cobbles derived from the Gangdese basement, and crosscutting dikes are early Miocene [*Harrison et al.*, 1993, 1998; *Ryerson et al.*, 1995]. The resulting inference is that significant denudation of the Gangdese batholith did not get underway until about 30 Ma, which in turn implies that the GT did not slip significantly until about that time.

5.3.2. Thermochronometry from the Dagze pluton. Approximately 40 km northwest of Zedong, three samples of granodiorite were earlier collected within the Dagze pluton

(Plate 1) at elevations of 5050 m, 3970 m, and 3440 m [*Pan*, 1993; *Pan et al.*, 1993]. The sample from the highest elevation yielded an apatite fission track date of 33±5 Ma, whereas samples from 3970 m and 3440 m gave identical ages of 19.1±2.1 and 20.2±1.6 Ma, respectively [*Pan et al.*, 1993]. The closure isotherm for fission tracks in apatite of ~110°C [*Naeser*, 1981] corresponds to a depth of ~4 km, assuming the geotherm described above. Thus these data constrain the ~110°C isotherm within the Dagze pluton between 33 to 20 Ma to have been located at a position that corresponds to a present elevation of 4500±500 m. Although such a simple calculation is unwise in a region undergoing rapid denudation due to advective compression of isotherms, these data imply a Peclet number ($U/\kappa z$) <<1 and thus our calculations are insensitive to this effect.

Given estimates of overburden removal at Zedong (i.e., ~13 km) and Dagze (~4 km), the magnitude of post 30 Ma differential denudation between these two locations is ~9 km. If we assume that this contrast is due to differential crustal thickening along a ramp-flat geometry (Figure 4), then the ~40 km that separate these two locations translates into a thrust ramp dip of 15°.

5.3.3. Region I thermochronometry. The K-feldspar thermal history results from the vertical traverse through the Yaja granodiorite (Plate 5) maybe used to constrain a thermal model that employs the above mentioned thrust geometry. In doing so, we consider only the seven samples from the Yaja massif (NM-1, NM-3 to NM-7, ZH-1-94; region I in Plate 2). We note, however, that the thermal history calculated for K-feldspar N-21 (Plate 4d), sampled ~8 km farther west, is indistinguishable from the Yaja results (Plates 4a-4c).

Thermal histories were recovered from $^{40}Ar/^{39}Ar$ stepheating results for K-feldspars from the top (NM-1), base (NM-7), and western side (ZH-1-94) of Yaja peak using the MDD model (Plates 4a-4c). Remarkably, results calculated for monotonic cooling and those that permit reheating define
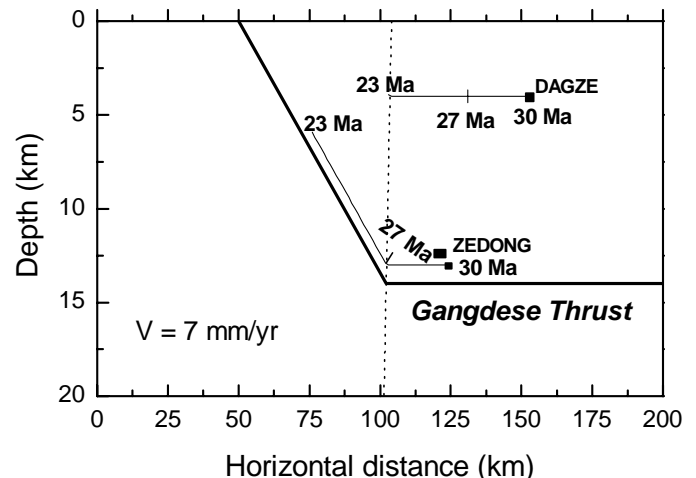

Figure 4. Projected cross-sectional representation of the numerical thermal model showing original and final positions of samples from the Yaja and Dagze plutons. Approximate starting sample positions are NM-1 = 2 km from the fault and 8 km from the vertex; NM-7 = 3 km from the fault and 8 km from the vertex; ZH-1-94 = 1 km from the fault and 10 km from the vertex.

essentially the same thermal history. All three results indicate rapid cooling (~80°C/Ma) from temperatures >375°C in the period 29-24 Ma (Plate 5). The weighted mean of seven biotite $^{40}Ar/^{39}Ar$ dates is 28.3±0.9 Ma (Table 1). Using the argon diffusion kinetics for biotite of *Grove and Harrison* [1996] ($E = 47.1 \pm 1.5$ kcal/mol; $D_o = 0.075^{+0.049}_{-0.021}$ cm^2/s), the effective diffusion radius ($r = 340$ μm) determined for a biotite from a Gangdese granodiorite [*Copeland et al.*, 1987], and the cooling rate indicated from the K-feldspar-derived thermal histories of ~80°C/Ma, a bulk biotite closure temperature of 360°C is calculated. This temperature-time datum is plotted together with the continuous K-feldspar thermal histories in Plate 5. The apatite fission track datum from *Yin et al.* [1994] is also shown.

5.3.4. Thermal modeling of slip on the Gangdese Thrust. The goal of forward thermal modeling presented below is to attempt to simultaneously match the cooling histories (Plate 4) of the Yaja massif and Dagze pluton 40 km to the north by varying slip rate. On the basis of the crystallization age of the Yaja granodiorite and the fact that the base of the pluton experienced synintrusive, high-temperature deformation, an initiation age of thrusting of 30 Ma is used in our thermal modeling calculations. As indicated in Figure 4, samples NM1, NM7, and ZH-1-94 K-feldspars were initially positioned between 11 and 13 km depth.

Forward modeling of the thermal history results from these samples constrains the time that the Yaja granodiorite samples began to move parallel to the ramp toward the surface at ~28 Ma. We found that the best fit to the cooling histories (Plate 5) is obtained for a slip rate of 7 mm/yr, with significant deviations occurring for values >50% faster or slower. Moving along the thrust at 7 mm/yr, all three locations rise from ~13 km to 3 to 5 km depth by 23 Ma. Note that this vertical positioning takes 2 km of topographic overburden produced by thrusting into account. Additional thermochronologic evidence supports hanging wall denudation occurring during this interval. Apatite fission track ages from structurally higher samples obtained just west of the Zedong Window at Samye (Plate 1) indicate rapid cooling there at 27-25 Ma [*Pan et al.*, 1993; *Copeland et al.*, 1995]. Both the K-feldspar thermal histories and apatite fission track results from the Zedong region [*Yin et al.*, 1994] and the Lhasa area to the north [*Pan et al.*, 1993; *Copeland et al.*, 1995] suggest that slip along the GT dramatically slowed or ceased after 23 Ma. These data are satisfied by either erosional decay of thrust-related topography and/or deceleration to a more modest slip rate (≤1 mm/yr) subsequent to 23 Ma.

5.4. Overprinting Due to the Renbu ZedongThrust

As indicated in Figure 3, $^{40}Ar/^{39}Ar$ thermochronological results from the strongly overprinted, eastern portion of the Zedong Window can be used to delineate two distinct regions that experienced somewhat different thermal histories (regions II and III in Plate 2). Monotonic cooling results derived from K-feldspar $^{40}Ar/^{39}Ar$ data from region II (including the YANS traverse as well as sample N-9) indicate rapid cooling from temperatures of ~300°C beginning at about 20 Ma (Plates 4j-4u). Solutions allowing reheating for region II (Plates 4j-4u) are quite variable at ages greater than about 20 Ma, but place firm controls on the interval between 20 and 15 Ma when temperatures were in the range of 250°C to 300°C. Note that, with the exception of YANS-11 (Plate 4r), the results from Region II all indicate that temperatures <200°C were attained by 15 Ma (see crosses in Plates 4a-4u). In con-trast, reheating results for region III (Plates 4e-4i) all indicate temperatures >200°C at 15 Ma. Thermal histories from region III (Plates 2 and 4j-4u) tend to show broad stable temperatures prior to about 15 Ma, whereas region II is characterized by increasing temperatures prior to that time (Plates 4e-4i). In contrast to region I, where cooling rates are ~80°C/Ma, cooling rates from peak temperature in both regions II and III are typically 20-5°C/Ma (Plates 4a-4c). The latter rates are characteristic of cooling due to erosional denudation, whereas the high rates from region I are more typical of fault-related refrigeration or tectonic denudation [*McDougall and Harrison*, 1999].

The thermal history results from region II are interpreted as reflecting slow cooling due to erosional denudation of a topographic high. If correct, the contrast in structural level between regions I and II must have been ~5 km as all samples from the NM traverse were between 150°C and 110°C at 20 Ma (Plate 5) when samples from region II varied from about 225°C to 300°C (Plates 4j-4u). Although the ~20 km distance over which this differential exposure occurred is sufficiently large to be due entirely to topography (i.e., region II was at an elevation 5 km higher than region I), variability of structural level of the GT could have resulted in significant oblique exposure along strike (i.e., the present exposure of the GT in region II was brought from greater depths than in region I). It remains unclear whether the high topography above this region at ~25 Ma was due to transport up the GT ramp or burial by the RZT. If the latter, the RZT must have been active at about 25 Ma. While this is earlier than previously documented [*Ratschbacher et al.*, 1994; *Quidelleur et al.*, 1997], no constraint known to us precludes such activity.

We interpret the temperature histories from region III as due to folding of GT hanging wall rocks during slip along the RZT. Note that in this region the GT dips steeply (75°) and is clearly warped west of sample N-14 (Plate 2). This interpretation is equivalent to model II of *Quidelleur et al.* [1997], in which heat advection due to deformation of the thrust hanging wall results in anomalously young ages close to the trace of the thrust. This model explains the uniformly higher temperatures in this region relative to region II (e.g., all temperatures >200° at 15 Ma).

Hornblende $^{40}Ar/^{39}Ar$ ages along a N-S traverse in the easternmost part of the study area vary from 44±4 Ma (N-13) to 38±2 Ma (N-11) to 30.8±1.0 (N-8) and to 30.5±0.4 Ma (N-9) (Table 1). The latter hornblendes (N-8 and N-9) are low K$_2$O amphiboles whose age spectra have been by contaminated by a less retentive, K-rich phase that is likely intergrown biotite. Given that the crystallization age for N-9 is established by U-Pb zircon dating at 48.9±0.4 Ma (Table 2), this age gradient suggests that N-8 and N-9 hornblendes experienced significant argon loss between 49 and 31 Ma (implying temperatures of >400°C during this interval), whereas sample N-13 did not. While this could reflect ~5 km of differential exposure across the GT hanging wall, opposite to that discussed above, we cannot rule out the thermal effect of possible nearby plutonism at about 30 Ma.

5.5. Significance of Granodiorite Crystallization Ages

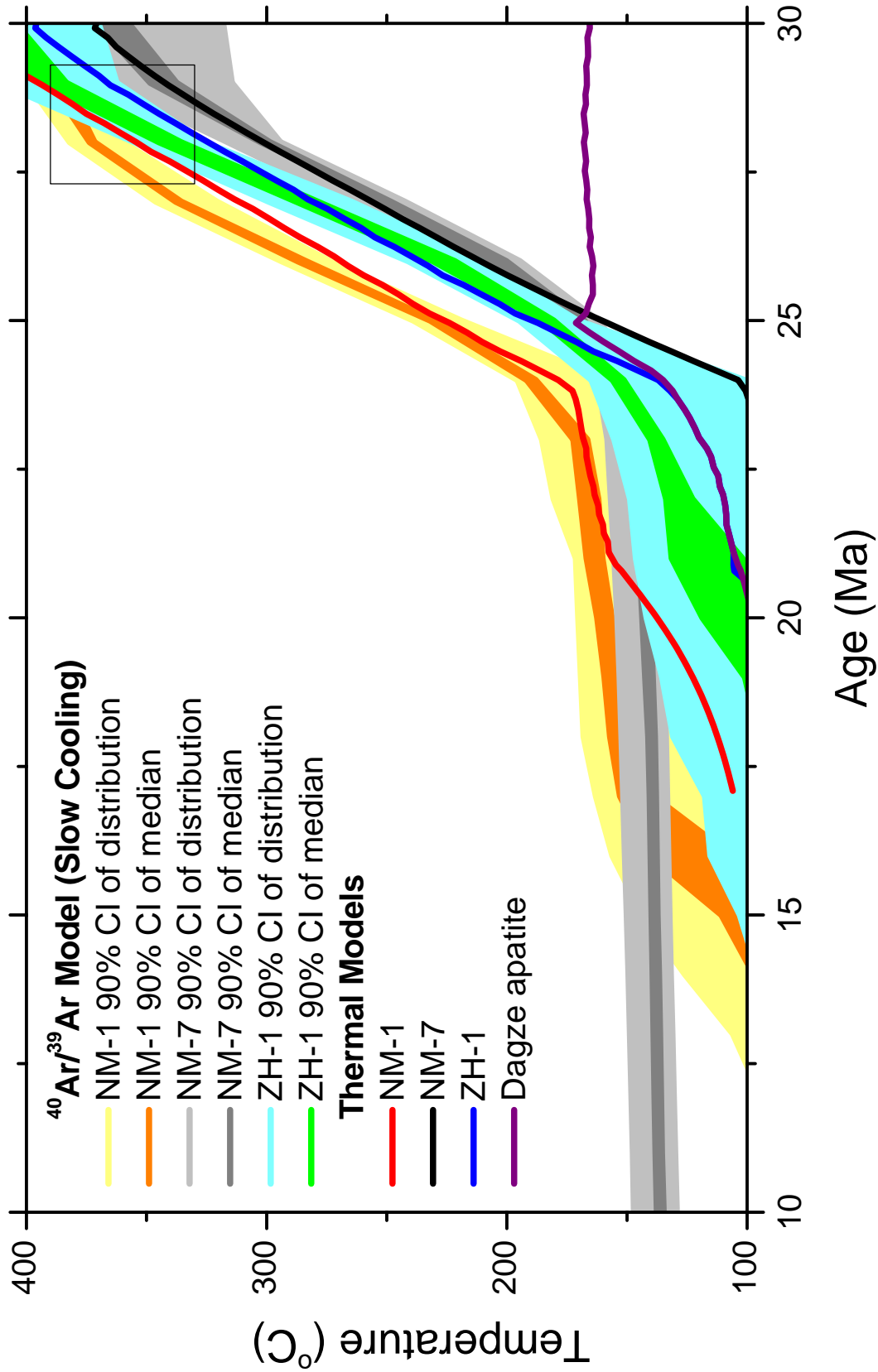Crystallization ages of the Kangagang-type granodiorite (42.5±1.0 Ma) and sample N-9 (48.9±0.4 Ma) are similar to

Plate 5. Thermal history results for the three samples from the Yaja granodiorite derived from ^{40}Ar/^{39}Ar step heating data of K-feldspar (CI is confidence interval). The average biotite age from the Yaja massif and its associated closure temperature is indi-cated by the box. Assuming that slip on the Gangdese Thrust begins at 30 Ma, a slip rate of 7 mm/yr fits these thermal history results. Also shown is the thermal history predicted for the 4500±500 m elevation of the Dagze pluton (see Plate 1 for location). The results are consistent with the 22 Ma apatite fission track ages observed at lower elevations in the Dagze pluton.

previously established ages for Gangdese plutons [*Honegger et al.*, 1982; *Schärer et al.*, 1984; *Copeland et al.*, 1995; *Yin et al.*, 1999]. Likewise, minimum crystallization ages yielded by hornblende $^{40}Ar/^{39}Ar$ ages from older granitoids in the GT hanging wall (N-25 = 66.6±0.5 Ma, N-5 = 64±3 Ma; Plate 2 and Table 1) that crop out west of Kangagang are in the age range of Gangdese magmatism elsewhere in the batholith [*Schärer et al.*, 1984; *Xu et al.*, 1985; *Coulon et al.*, 1986; *Pan*, 1993; *Quidelleur et al.*, 1997]. The comparative youth of the Yaja granodiorite at 30.4±0.4 Ma, however, merits further discussion.

The Yaja granodiorite does not represent the youngest arc-type magmatism in the Gangdese belt. High-K, calc-alkaline volcanism with geochemical affinity to the Gangdese belt has been documented at 18-16 Ma in southeastern Tibet [*Miller et al.*, 1999] (Plate 1) and at 16-10 Ma near Maquiang [*Coulon et al.*, 1986] (Plate 1). While it has been possible to view these Miocene volcanics as representing a fundamentally different petrogenetic process than that responsible for the batholith [*Turner et al.*, 1993], discovery of a 30 Ma Gangdese granodiorite opens the possibility that a continuous process produced calc-alkaline magmatism throughout the Tertiary.

Paleontologic evidence indicates that India had impinged upon Asia by ~55 Ma [*Gaetani and Garzanti*, 1991; *Beck et al.*, 1995], and possibly as early as 64 Ma [*Willems et al.*, 1996; *Shi et al.*, 1996; *Jaeger et al.*, 1989[(see review of *Yin and Harrison* [2000]). Thus fluid and thermal conditions remained appropriate for magmatism characteristic of arc settings for ~50 million years after subduction of oceanic lithosphere ceased. Indeed, worldwide, arc magmatism is observed to occur subsequent to the cessation of oceanic subduction [*Pearce et al.*, 1984; *Metcalfe and Smith*, 1995; *Muir et al.*, 1995]. Thus it would seem ill-advised to use the presence of arc-type magmatism as an indicator of active subduction of oceanic lithosphere beneath a continental margin [e.g., *Schärer et al.*, 1984; *Dewey et al.*, 1988; *Ernst*, 1999].

There are several possible mechanisms that could potentially explain middle Eocene to middle Miocene calc-alkaline magmatism in southern Tibet including (1) melting of Asian mantle lithosphere, metasomatized during the earlier phase of oceanic subduction, in response to asthenospheric upwelling associated with break-off of the oceanic slab [e.g., *Davies and von Blanckenburg*, 1995], (2) melting due to fluid influx from dehydrating continental crust (+flysch) underthrust beneath Asian mantle lithosphere, and (3) postsubduction melting of mafic lower crust (± mantle lithosphere). In its simplest form, model 1 predicts a single episode of postcollisional (i.e., <55 Ma) melting, whereas our challenge is to explain semicontinuous calc-alkaline magmatism from about 55 to 10 Ma. Model 2 is consistent with the magmatic history but contradicts recent reconstructions of the tectonic evolution of southern Tibet which assume direct contact between the Indian craton and Asian crust during the Neogene [e.g., *Nelson et al.*, 1996; *Owens and Zandt*, 1997]. The near continuous generation of calc-alkaline magmatism is also consistent with melting of gabbroic material (generated during mafic underplating accompanying the earlier phase of subduction) or thermally reequilibrated oceanic crust abandoned following subduction. Fluids necessary to instigate postcollisional melting could have been stored in the source region or been introduced during continental subduction. Permissive evidence of the latter is that no postcollisional calc-alkaline magmatism has yet been documented adjacent

to the central part of the Gangdese belt where the Xigaze flysch has not been overridden (Plate 1).

If the Indian craton has been continually underthrust beneath Asia since the disappearance of the Tethyan oceanic lithosphere, then the Asian lower crust and/or mantle lithosphere would have experienced significant refrigeration. For melting to have been induced under these circumstances requires that a source of thermal energy be present, at least locally, for over 40 million years. There is evidence for transient inputs of significant heat into southern Tibet in that some Neogene crustal melts experienced peak temperatures in excess of 800°C [*D'Andrea et al.*, 1999] while the steady state Moho temperature beneath southern Tibet is estimated at <750°C [*Ruppel and McNamara*, 1997]. These observations appear to require involvement of asthenospheric heat, possibly following repeated slab break off [e.g., *Pysklywec et al.*, 1999], rollback of delaminated Indian mantle lithosphere [*Bird*, 1978; *Van der Voo et al.*, 1999], or melts ascending via extension in the overlying plate margin caused by oblique subduction [e.g., *Debon et al.*, 1986].

6. Conclusions

The south directed Gangdese Thrust System (GTS) is exposed near Zedong, southeastern Tibet, in a structural window created where the trace of back thrusts belonging to the younger north directed Renbu Zedong Thrust System (RZTS) were displaced south of the suture zone. Zircon U-Pb ages and $^{40}Ar/^{39}Ar$ dates from hornblende, biotite, and K-feldspar from granitoids samples in the central portion of the Zedong Window constrain the slip history of the Gangdese Thrust. U-Pb zircon dating of three samples of the Yaja granodiorite, a hanging wall pluton cut by the GT, yields a crystallization age of 30.4±0.4 Ma. Combined with field relations, this result establishes an upper bound on initiation of the GT mylonite zone. Geochemical data show that this pluton is petrogenetically similar to precollisional elements of the Gangdese batholith, implying a significant postcollisional input of juvenile heat to produce calc-alkaline magmatism. The $^{40}Ar/^{39}Ar$ thermochronology of samples from a vertical section through the Yaja granodiorite indicate rapid cooling beginning at about 27 Ma. Assuming that this cooling event reflects motion of the hanging wall up the thrust ramp, these and other thermochronological data were used to constrain a numerical thermal model of fault evolution. A good fit between the thermochronological data and model results was obtained assuming a slip rate along the GT of 7 mm/yr between 30 and 23 Ma. Thus the minimum displacement on the GT is ~50 km.

In the eastern portion of the Zedong Window, early Miocene topography north of the GT, either due to crustal thickening along the GT or burial by backthrusting by the RZTS, maintained warmer conditions within the GT hanging wall than farther west. Two thermal regimes are recognized; a northern region in which temperatures were <200°C at 15 Ma and a southerly region where temperatures were well in excess of 200°C at 15 Ma. The thermal conditions in the eastern part of the Zedong Window obscure the earlier history related to the Gangdese Thrust.

U-Pb zircon dating of samples from the Kangagang granodiorite, higher in the hanging wall than the Yaja pluton, yields a crystallization age of 42.5±1.0 Ma. While this is similar to emplacement ages of plutons elsewhere in the Gangdese batholith (e.g., Quxu, Kailas), the 30 Ma age of the

Yaja pluton is significantly younger than previous estimates for the termination of subduction of oceanic lithosphere. It is apparent that calc-alkaline magmatism can continue many ten's of millions of years following continent-continent collision and is thus a poor indicator of the timing of active subduction of oceanic lithosphere beneath a continental margin. The thermal energy required to overcome the continued refrigeration of Asian lower crust by the underthrusted Indian craton appears to reflect asthenospheric involvement, possibly in the form of melts ascending via extension in the overlying plate margin caused by oblique subduction, by repeated slab break off, or rollback of delaminated Indian mantle lithosphere. Fluids necessary to instigate melting may have been introduced during continental subduction.

References

Allegre, C.J., et al., Structure and evolution of the Himalaya-Tibet orogenic belt, *Nature*, *307*, 17-22, 1984.

Beck, R.A., et al., Stratigraphic evidence for an early collision between northwest India and Asia, *Nature*, *373*, 55-58, 1995.

Bird, P., Initiation of intracontinental subduction in the Himalaya, *J. Geophys. Res.*, *83*, 4975-4987, 1978.

Burg, J. P. (Compiler), Carte Geologique du Sud du Tibet, scale, 1:500,000, Cent. Natl. de la Rech. Sci., Paris, 1983.

Chang, C., et al., Preliminary conclusions of the Royal Society and Academia Sinica 1985 geotraverse of Tibet, *Nature*, *323*, 501-507, 1986.

Cheng, J., and G. Xu, Geologic map at a scale of 1:1,000,000 and geologic report of the Gedake region, Tibetan Bureau of Geology and Mineral Resources, 363 pp., 1987.

Copeland, P., T.M. Harrison, W.S.F. Kidd, X. Ronghua, and Z. Yuquan, Rapid early Miocene acceleration of uplift in the Gandese Belt, Xizang-southern Tibet, and its bearing on accommodation mechanisms of the India-Asia collision, *Earth Planet. Sci. Lett.*, *86*, 240-252, 1987.

Copeland, P., T.M. Harrison, Y. Pan, W.S.F. Kidd, M. Roden, and Y. Zhang, Thermal evolution of the Gangdese batholith, southern Tibet: A history of episodic unroofing, *Tectonics*, *14*, 223-236, 1995.

Coulon, C., H. Maluski, C. Bolling, and S. Wang, Mesozoic and Tertiary rocks from central and southern Tibet: $^{40}Ar/^{39}Ar$ dating, petrologic characteristics and geodynamic significance, *Earth Planet. Sci. Lett.*, *79*, 281-302, 1986.

Crank, J., *The Mathematics of Diffusion*, 2nd ed., Clarendon , Oxford, England, 1975.

Dalrymple, G.B., M. Grove, O.M. Lovera, T.M. Harrison, J.B. Hulen, and M.A. Lanphere, Age and thermal history of the Geysers Plutonic Complex (Felsite Unit), Geysers Geothermal Field, California, *Earth Planet. Sci. Lett.*, *173*, 285-298, 1999.

D'Andrea, J., T.M. Harrison, and M. Grove, The post-collisional thermal and compositional structure of the Gangdese Arc, Nyainqentanglha, Southern Tibet, Eos, Trans. AGU 80 (46), Fall Meet. Suppl., F991, 1999.

Davies, J.H., and F. von Blanckenburg, Slab breakoff–A model of lithosphere detachment and its test in the magmatism and deformation of continental orogens, *Earth Planet. Sci. Lett.*, *129*, 85-102, 1995.

Debon, F., P. Le Fort, S.M.F. Sheppard, and J. Sonet, The four plutonic belts of the Transhimalaya–Himalaya: A chemical, mineralogical, isotopic, and chronological synthesis along a Tibet–Nepal section, *J. Petrol.*, *21*, 219-250, 1986.

Dewey, J.F., R.M. Shackleton, C. Chang, and Y. Sun, The tectonic evolution of the Tibetan Plateau, *Philos. Trans. R. Soc. London, Ser. A, 327*, 379-413, 1988.

England, P., and D. McKenzie, A thin viscous sheet model for continental deformation, *Geophys. J. R. Astron Soc.*, *70*, 295-321, 1982.

England, P., and M.P. Searle, The Cretaceous–Tertiary deformation of the Lhasa block and its implications for crustal thickening in Tibet, *Tectonics, 5*, 1–14, 1986.

Ernst, W.G., Hornblende, the continent maker–Evolution of H_2O during circum-Pacific subduction versus continental collision, *Geology*, *27*, 675-678, 1999.

Faure, G., *Principles of Isotope Geology*, 2nd ed., 589 pp., John Wiley, New York, 1986.

Gaetani, M., and E. Garzanti, Multicyclic history of the northern India continental margin (northwest Himalaya), *AAPG Bull.*, *75*, 1427-1446, 1991.

Gansser, A., *The Geology of the Himalayas*, 289 pp., Wiley-Interscience, New York, 1964.

Grove, M., and T.M. Harrison, ^{40}Ar diffusion in Fe-rich biotite, *Am. Mineral.*, *81*, 940-951, 1996.

Harrison, T.M., O.M. Lovera, and M.T. Heizler, $^{40}Ar/^{39}Ar$ results for multi-domain samples with varying activation energy, *Geochim. Cosmochim. Acta, 55*, 1435-1448, 1991.

Harrison, T.M., P. Copeland, W.S.F. Kidd, and A. Yin, Raising Tibet, *Science*, *255*, 1663-1670, 1992.

Harrison, T.M., P. Copeland, S.A. Hall, J. Quade, S. Burner, T.P. Ojha, and W.S.F. Kidd, Isotopic preservation of Himalayan/Tibetan uplift, denudation, and climate histories of two molasse deposits, *J. Geol., 100*, 157-175, 1993.

Harrison, T.M., P. Copeland, W.S.F. Kidd, and O.M. Lovera, Activation of the Nyainqentanghla shear zone: Implications for uplift of the southern Tibetan Plateau, *Tectonics, 14*, 658-676, 1995.

Harrison, T. M., F. J. Ryerson, P. Le Fort, Yin, A.,O. M. Lovera, and E.J. Catlos, A late Miocene-Pliocene origin for the Central Himalayan inverted metamorphism, *Earth Planet. Sci. Lett., 146*, E1-E8, 1997a.

Harrison, T. M., O. M. Lovera, and M. Grove, New insights into the origin of two contrasting Himalayan granite belts, *Geology, 25*, 899-902, 1997b.

Harrison, T. M., M. Grove, O. M. Lovera, and E. J. Catlos, A model for the origin of Himalayan anatexis and inverted metamorphism, *J. Geophys. Res., 103*, 27,017-27,032, 1998.

Heim, A., and A. Gansser, Central Himalaya, geological observations of the Swiss expedition 1936, *Mem. Soc. Helv. Sci. Nat., 63*, 1939.

Henry, S.G., and H.N. Pollack, Terrestrial heat flow above the Andean subduction zone, Bolivia and Peru, *J. Geophys. Res., 93*, 15,153-15,162, 1988.

Honegger, K., Dietrich, W. Frank, A. Gansser, M. Thoni, and V. Trommsdorff, Magmatism and metamorphism in the Ladakh Himalayas (the Indus-Tsangpo suture zone), *Earth Planet. Sci. Lett., 60*, 253-292, 1982.

Houseman, G.A., D.P. McKenzie, and P. Molnar, Convective instability of a thickened boundary layer and its relevance for the thermal evolution of continental convergent belts, *J. Geophys. Res., 86*, 6115-6132, 1981.

Jaeger, J.-J., V. Courtillot, and P. Tapponnier, Paleontological view of the ages of the Deccan traps, the Cretaceous/Tertiary boundary and the Indo-Asian collision, *Geology*, *17*, 316-319, 1989.

Kidd, W.S.F., Y. Pan, C. Chang, M.P. Coward, J.F. Dewey, A. Gansser, P. Molnar, R.M. Shackleton, and Y. Sun, Geologic mapping of the 1985 Chinese-British (Xizang-Qinghai) Geotraverse route, *Philos. Trans. R. Soc. London, Ser. A, 327*, 287-305, 1988.

Liu, Z.Q. (Compiler), Geologic map of the Qinghai-Xizang Plateau, scale, 1:5,000,000, Chengdu Inst. Geol. Miner. Resour., Chin. Acad. Geol. Sci., Geol. Publ. House, Beijing, 1988.

Lovera, O.M., F.M. Richter, and T.M. Harrison, $^{40}Ar/^{39}Ar$ geothermometry for slowly cooled samples having a distribution of diffusion domain sizes, *J. Geophys. Res., 94*, 17,917–17,935, 1989.

Lovera, O.M., M. Grove , T.M. Harrison, and K.I. Mahon, Systematic analysis of K-feldspar $^{40}Ar/^{39}Ar$ step-heating experiments, I, Significance of activation energy determinations, *Geochim. Cosmochim. Acta, 61*, 3171-3192, 1997.

Makovsky, Y., S. Klemperer, L. Huang, and D. Lu, Structural elements of the southern Tethyan Himalaya crust from wide-angle seismic data, *Tectonics*, *15*, 997-1005, 1996.

McDougall, I., and T.M. Harrison, *Geochronology and Thermochronology by the $^{40}Ar/^{39}Ar$ Method*, 2nd ed., 261 pp., Oxford Univ. Press, New York, 1999.

Metcalfe, R.V., and E.I. Smith, Introduction to special section: Magmatism and extension, *J. Geophys. Res.*, *100*, 10,249-10,253, 1995.

Miller, C., R. Schuster, U. Klötzli, W. Frank, and F. Purtscheller, Post-collisional potassic and ultrapotassic magmatism in SW Tibet: Geochemical and Sr-Nd-Pb-O isotopic constraints for mantle source characteristics and petrogenesis, *J. Petrol.*, *40*, 1399-1424, 1999.

Muir, R.J., S.D. Weaver, J.D. Bradshaw, G.N. Eby, and J.A. Evans, The Cretaceous Separation Point Batholith, New Zealand–Granitoid magmas formed by melting of mafic lithosphere, *J. Geol. Soc.*, *152*, 689-701, 1995.

Murphy, M.A., A. Yin, T.M. Harrison, S.B. Durr, Z. Chen, F.J. Ryerson, W.S.F. Kidd, X. Wang, and X. Zhou, Did the Indo-Asian collision alone create the Tibetan plateau?, *Geology*, *25*, 719-722, 1997.

Naeser, C.W., The fading of fission tracks in the geologic environment–data from deep drill holes, *Nucl. Tracks*, *5*, 248-258, 1981.

Nelson, K.D., et al., Partial molten middle crust beneath southern Tibet: Synthesis of Project INDEPTH results, *Science*, *274*, 1684-1687, 1996.

Owens, T.J., and G. Zandt, Implications of crustal property variations for models of Tibetan plateau evolution, *Nature*, *387*, 37-43, 1997.

Paces, J.B., and J.D. Miller, Precise U-Pb age of Duluth Complex and related mafic intrusions, northeastern Minnesota: Geochronological insights into physical, petrogenetic, paleomagnetic, and tectonomagmatic processes associated with the 1.1 Ga midcontinent rift system, *J. Geophys. Res., 98*, 13,997-14,013, 1993.

Pan, Y., Unroofing history and structural evolution of the southern Lhasa Terrane, Tibetan plateau: Implications for the continental collision between India and Asia, Ph.D. thesis, 395 pp., State Univ. of N.Y., Albany, 1993.

Pan, Y., P. Copeland, M.K. Roden, W.S.F. Kidd, and T.M. Harrison, Thermal and unroofing history of the Lhasa area, southern Tibet–Evidence from apatite fission track thermochronology, *Nucl. Tracks Radiat. Meas.*, *21*, 543-554, 1993.

Pearce, J.A., N.B.W. Harris, and A.G. Tindle, Trace element discrimination diagrams for the tectonic interpretation of granitic rocks, *J. Petrol.*, *25*, 956-983, 1984.

Pysklywec, R.N., C. Beaumont, and P. Fullsack, Using thermochemical models to investigate the Fate of the Mantle-lithosphere During Plate Convergence, Eos, Trans. AGU 80 (46), Fall Meet. Suppl., F949, 1999.

Quidelleur, X., M. Grove, O.M. Lovera, T. M. Harrison, A. Yin, and F.J. Ryerson, Thermal evolution and slip history of the Renbu-Zedong thrust, southeastern Tibet, *J. Geophys. Res.*, *102*, 2659-2679, 1997.

Ratschbacher, L., W. Frisch, G. Liu, and C.C. Chen, Distributed deformation in southern and western Tibet during and after the India-Asia collision, *J. Geophys. Res.*, *99*, 19,917-19,945, 1994.

Ruppel, C., and D.E. McNamara, Seismic and rheological constraints on the thermal state of Tibetan Plateau upper mantle: Implications for melt production, mantle delamination, and large-scale tectonics, Eos, Trans. AGU 78 (46), Fall Meet. Suppl., F650, 1997.

Ryerson, F.J., A. Yin, T.M. Harrison, and M.A. Murphy, The Gangdese and Renbu Zedong thrust systems: Westward extension to Mt. Kailas, *Geol. Soc. Am. Abstr. Programs*, *27*, A335, 1995.

Schärer, U., R.H. Xu, and C.J. Allègre, U-Pb geochronology of the Gangdese (Transhimalaya) plutonism in the Lhasa-Xigaze region, Tibet, *Earth Planet. Sci. Lett.*, *69*, 311-320, 1984.

Searle, M.P., et al., The closing of Tethys and the tectonics of the Himalaya, *Geol. Soc. Am. Bull.*, *98*, 678-701, 1987.

Shi, X., C. Zhao, and C. Jia, Mesozoic to Cenozoic sequence stratigraphy and sea-level changes in the northern Himalaya, southern Tibet, China, *Newsl. Stratigr.*, 33, 15-61, 1996.

Tibetan Bureau of Geology and Mineral Resources, *Geology of the Xizang Autonomous Region*, 707 pp., Beijing, 1982.

Turcotte, D.L., and G. Schubert, *Geodynamics: Applications of Continuum Physics to Geological Problems*, 450 pp., John Wiley, New York, 1982.

Turner, S., C. Hawkesworth, J. Liu, N. Rogers, S. Kelley, and P. van Calsteren, Timing of Tibetan uplift constrained by analysis of volcanic rocks, *Nature, 364*, 50–54, 1993.

Van der Voo, R., W. Spakman, and H. Bijwaard, Tethyan subducted slabs under India, *Earth Planet. Sci. Lett., 171*, 7-20, 1999.

Wang, S., Z. Li, and X. Qiangba, Geologic map (1:1,000,000) and geologic report of the Xigaze area, Tibetan Bur. Geol. Miner. Resour., 568 pp., Beijing, 1983.

Willems, H., Z. Zhou, B. Zhang, and K.U. Grafe, Stratigraphy of the Upper Cretaceous and Lower Tertialy strata in the Tethyan Himalaya of Tibet (Tingri area, China), *Geol. Rundsh.*, *85*, 723-754, 1996.

Xu, R., Geochronological study of granitoids and metamorphic rocks in Xizang, in *Metamorphic and Igneous Rocks in Xizang*, edited by G. Lui et al., pp. 287-321, Geol. Press, Beijing, 1990.

Xu, R.-H., U. Schärer, C.J. Allègre, Magmatism and metamorphism in the Lhasa block (Tibet): a geochronological study, *J. Geol.*, *93*, 41-57, 1985.

Yin, A., and T.M. Harrison, Geologic evolution of the Himalayan-Tibetan Orogen, *Annu. Rev. Earth Planet. Sci.*, in press, 2000.

Yin, A., T.M. Harrison, F.J. Ryerson, W.J. Chen, W.S.F. Kidd, P. Copeland, and W. Chen, The Gangdese Thrust revealed, Eos, Trans. AGU 73 (43), Fall Meet. Suppl., 545, 1992.

Yin, A., T.M. Harrison, F.J. Ryerson, W.J. Chen, W.S.F. Kidd, and P. Copeland, Tertiary structural evolution of the Gangdese thrust system in southeastern Tibet, *J. Geophys. Res., 99*, 18,175-18,201, 1994.

Yin, A., T.M. Harrison, M.A. Murphy, M. Grove, S. Nie, F.J. Ryerson, Wang X.F., and Z.L. Chen, Tertiary deformation history of southeastern and southwestern Tibet during the Indo-Asian collision, *Geol. Soc. Am. Bull.*, 111, 1-21, 1999.

Yu, Z., and A. Zheng, Geologic Map of the Lhasa region at a scale of 1:1,000,000, Geol. Publ. House, Beijing, 1979.

M. Grove, T. M. Harrison, O. M. Lovera, and A. Yin, Department of Earth and Space Sciences, University of California, Los Angeles, CA 90095-1567. (tmh@argon.ess.ucla.edu; yin@ess.ucla.edu; marty@argon.ess.ucla.edu; lovera@argon.ess.ucla.edu)

F. J. Ryerson, Lawrence Livermore National Laboratory, Livermore, P.O. Box 808, Livermore, CA 94602 (ryerson@llnl.gov)

X. Zhou, Academia Sinica, Institute of Geology, 100029, Beijing, China (zhouxh@public3.bta.net.cn)